Phase Stability

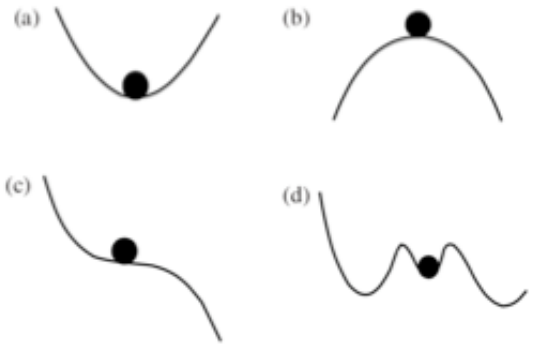

Figure 5.5 Ball in a gravitational field; illustration of (a) stable, (b) unstable, (c) spinodal and (d) metastable equilibria.

Supercool/Superheat/Supersaturate

At the equilibrium melting/freezing point or equilibrium concentration for precipitation the driving force for phase separation, $\Delta G = \Delta H - T\,\Delta S = 0$. So, a phase will only form by lowering the temperature below the melting point or increasing the concentration above the solubility limit. This is related to "critical slowing down". At the critical point nothing happens, or anything can happen, there is no thermodynamic direction for the process.

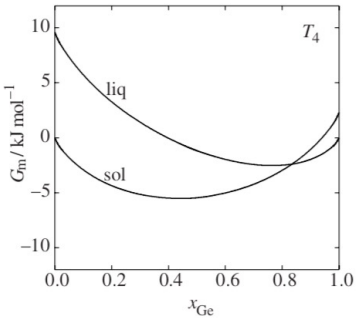

Cooling below the melting point produces a supercooled liquid, raising the concentration above the saturation limit produces a supersaturated solution. You can also heat a solid above the equilibrium melting point and produce a superheated solid.

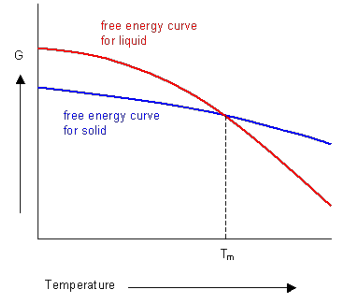

The rate of phase separation depends on two factors:
ΔG and kinetics. Kinetics slows exponentially at lower temperatures $D \sim \exp(K/(T-T_0))$. The thermodynamic driving force, $\exp(-\Delta G/kT)$, decays at higher temperatures, so a maximum in growth rate results below the equilibrium in the super cooled liquid state.

$$\Delta G = \Delta H - T\,\Delta S$$

Supercool/Superheat/Supersaturate

The rate of phase separation depends on two factors:
ΔG and kinetics. Kinetics slows exponentially at lower temperatures $D \sim \exp(K/(T-T_0))$. The thermodynamic driving force, $\exp(-\Delta G(T)/kT)$, decays at higher temperatures, so a maximum in growth rate results below the equilibrium in the super cooled liquid state.

To homogeneously form a crystal, you need to 1) form a nucleus or seed then 2) grow from the seed. At deep quench you get a lot of seeds but slow growth since transport is slow. At high temperature you see few seeds, but the kinetics are fast.

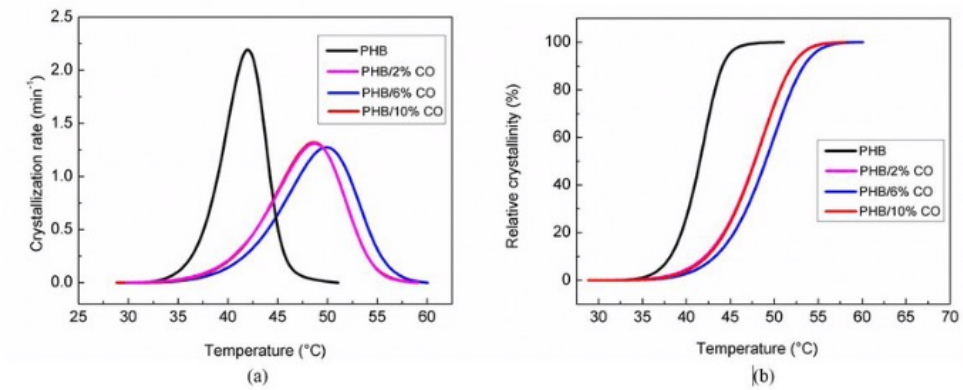

(a) Graph of the crystallization rate versus temperature of PHB film and PHB/CO films with different compositions; (b) Graph of the relative crystallinity versus temperature of PHB film and PHB/CO films with different compositions.

Evaluation of the mechanical and thermal properties of PHB/canola oil films

Article | Full-text available | Sep 2017

Cláudia Daniela Melo Giaquinto · Grasielly Souza · Viviane Caetano · Glória Maria Vinhas

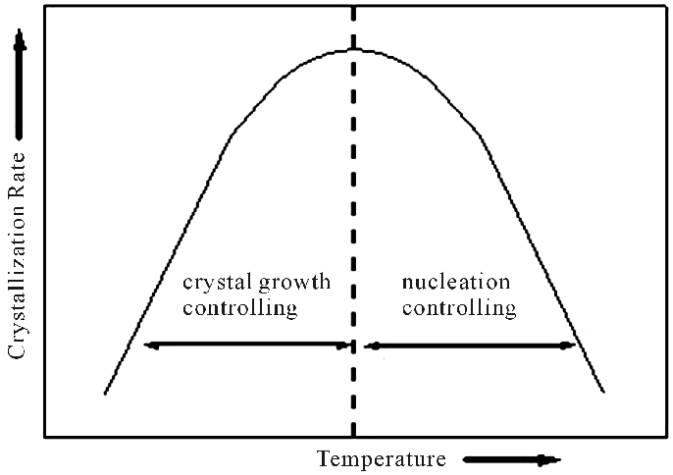

Kauzmann Paradox, a thermodynamic basis for the glass transition

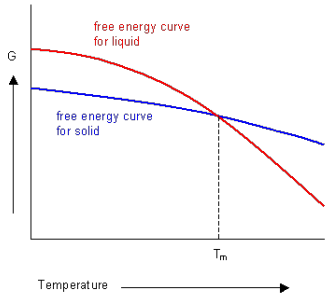

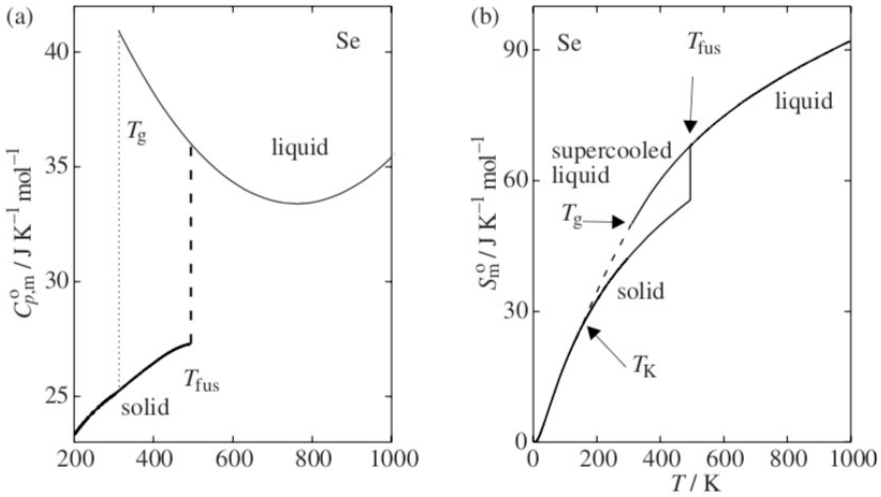

Figure 5.1 (a) Heat capacity of crystalline, liquid and supercooled liquid Se as a function of temperature [1–3]. (b) Entropy of crystalline, liquid and supercooled liquid Se as a function of temperature.

$$\Delta_{fus} S^o_m(T) = \Delta_{fus} S^o_m(T_{fus}) + \int_{T_{fus}}^{T} \frac{\Delta C^o_p}{T} dT$$

The entropy of the liquid becomes smaller than the entropy of the solid at the Kauzmann temperature, T_K. This could be the infinite cooling glass transition temperature.

Selenium like sulfur can form chain molecules
Selenium forms a hexagonal crystal of helical chains (slow kinetics)

Superheating and Melting

Superheating can occur since melting occurs at surfaces and if the surfaces are stabilized then superheated solids can be produced

Growth of a liquid phase relies on growth of a mechanical instability

A mechanical instability will not spontaneously grow if it occurs in a meta-stable region in T and P:

$(dG/dx)=0$ defines equilibrium or binodal; $(d^2G/dx^2) = 0$ defines the metastable limit or spinodal

$(d^3G/dx^3) = 0$ defines the critical point

$dG = -SdT + Vdp$

Metastable region defined by

$(d^2G/dp^2)_T = (dV/dp)_T < 0$ and $(d^2G/dT^2)_p = -(dS/dT)_p < 0$

First requires that the bulk modulus be positive, $K_T = \frac{1}{\kappa_T} = -\frac{V}{(\partial V / \partial p)_T} > 0$

Second requires positive heat capacity, $(dS/dT)_p = C_p/T > 0$

-S U V

H A

-p G T

$933K = T_{m,Al}$

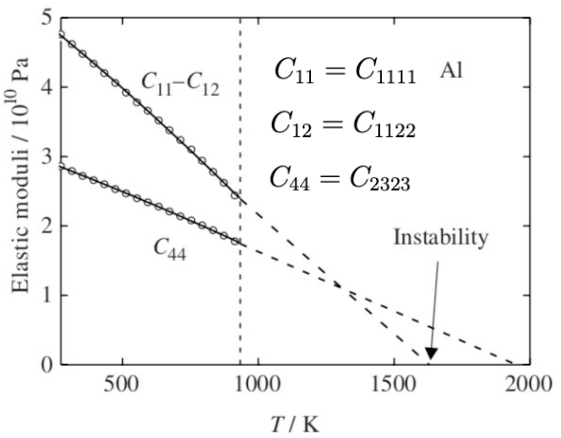

Shear modulus goes to 0 at highest possible supercritical solid

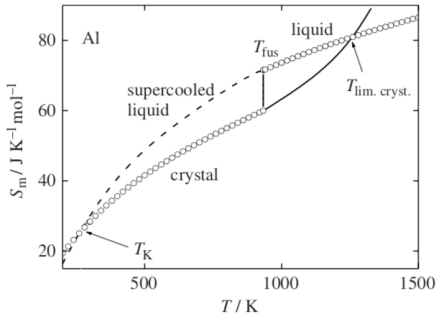

Figure 5.3 Entropy of liquid and crystalline aluminium in stable, metastable and unstable temperature regions [12]. The temperatures where the entropy of liquid and crystalline aluminium are equal are denoted T_K and $T_{\text{lim cryst}}$, respectively.

Figure 5.2 Temperature dependence of the isothermal elastic stiffness constants of aluminium [10].

Thermal (energy) fluctuations are the basis of thermodynamics

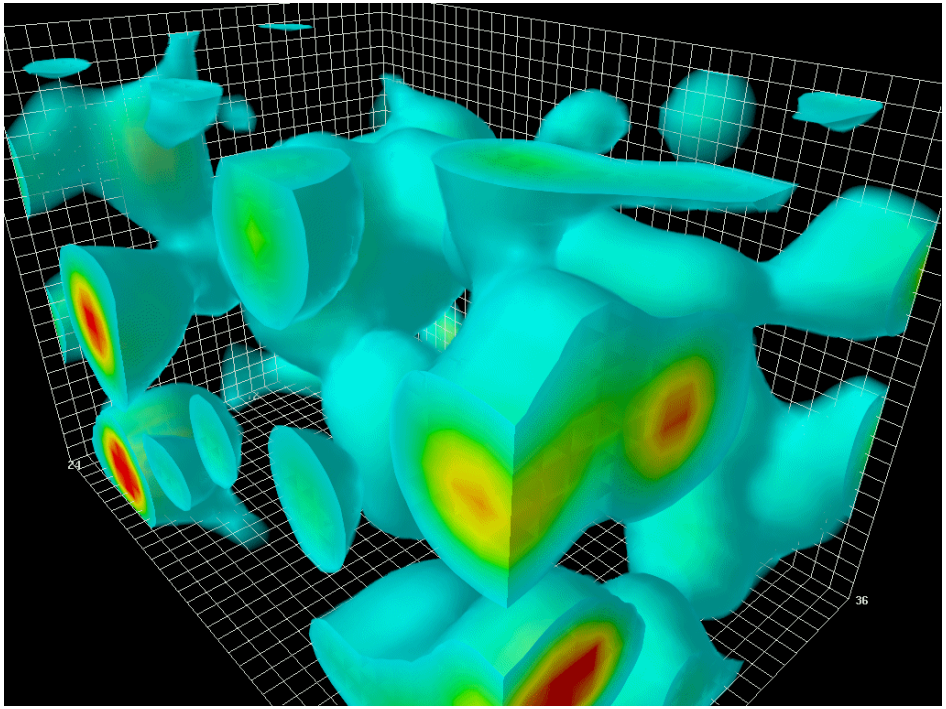

Map of energy in 3d space at one time slice

https://upload.wikimedia.org/wikipedia/commons/2/2a/Quantum_Fluctuations.gif

Thermodynamic Hypothesis:

Systems are always probing free energy space (temperature, composition, pressure, magnetic field, electrical field, energy, extent of reaction, etc.) through random fluctuations. This enables the attainment of the lowest free energy at an equilibrium state.

This hypothesis leads to consideration of the partial derivatives of free energy as defining features in free energy space particularly critical points ($d^3G/dx^3=0$; $d^2G/dx^2=0$; $dG/dx=0$), equilibrium (binodal) points ($dG/dx=0$), and spinodal points ($d^2G/dx^2=0$).

The book considers first a reversible chemical reaction A <=> B
Cyclohexane from boat to chair conformation for instance

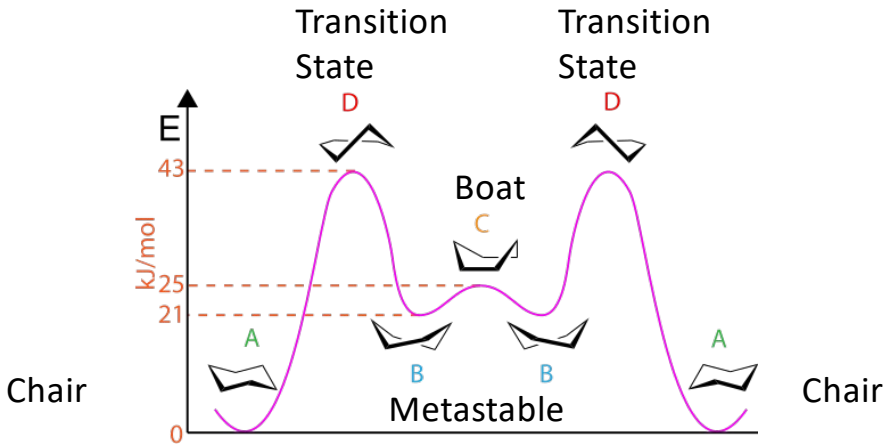

The equilibrium point depends on temperature, k_BT

As temperature changes you can observer a different mix of states, $E = k_BT \sim 2.5$ kJ/mole at RT
But fluctuations allow for 0.1 % boat conformation. At 1073K 30% boat. Probability is exp(-E/kT).
The percent in boat can be measured using NMR spectroscopy.

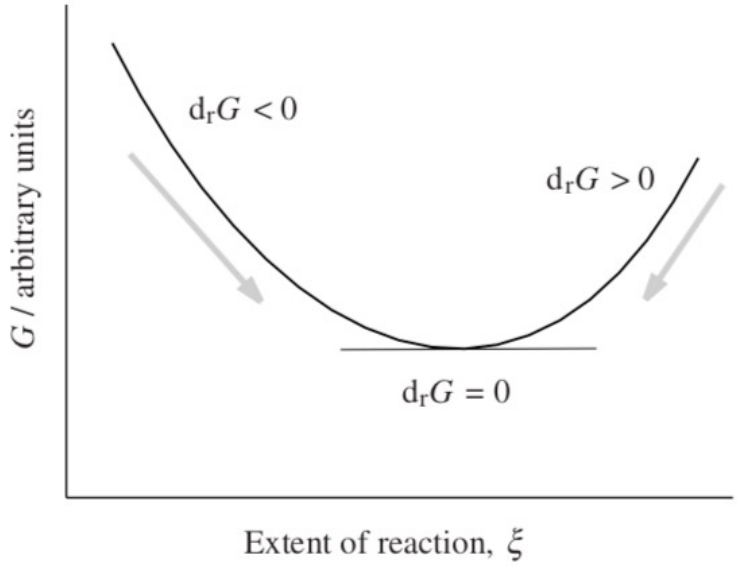

Figure 5.4 Gibbs energy as a function of the extent of reaction.

Extent of reaction would be the conversion from chair (A) to boat (B), for instance, at a temperature T. The minimum, $(dG/d\xi) = 0$ is the equilibrium point. The free energy plot can be concave up (stable equilibrium) concave down (unstable), flat (critical point/temperature), and other shapes

A <=> B

$$-dn_A = dn_B = d\xi$$

$$d_rG = \mu_A dn_A + \mu_B dn_B = -\mu_A d\xi + \mu_B d\xi = (\mu_B - \mu_A)d\xi$$

$$A_k = \mu_A - \mu_B \quad \text{Affinity}$$

At temperature T, the reaction is like a spring bouncing between A and B oscillating about the equilibrium point since any deviation from equilibrium increases the free energy.

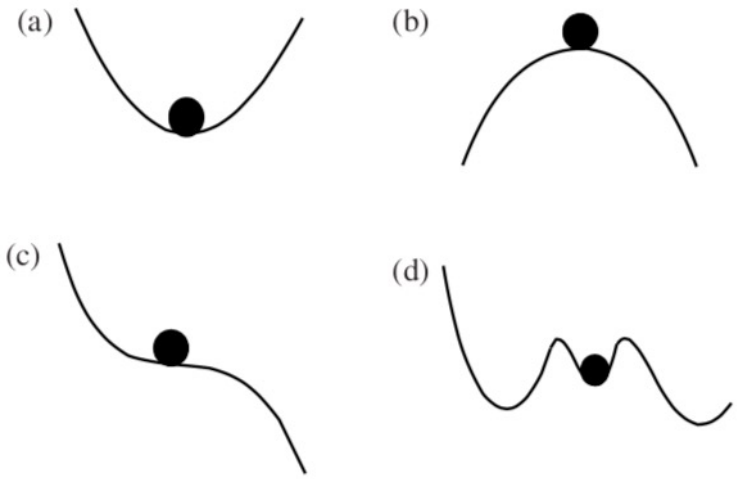

Figure 5.5 Ball in a gravitational field; illustration of (a) stable, (b) unstable, (c) spinodal and (d) metastable equilibria.

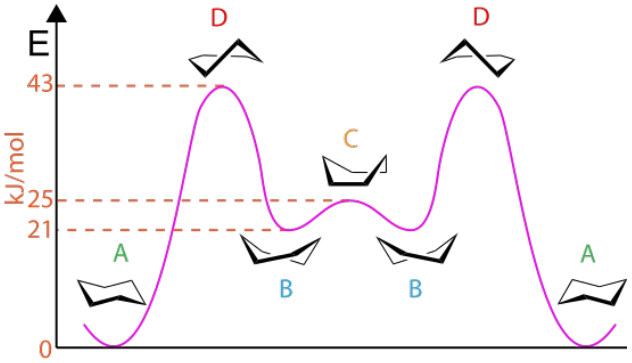

a) Stable $dG/dx = 0$
b) Unstable
c) Spinodal $d^2G/dx^2 = 0$
d) Metastable (This can depend on your vantage point)

Affinity as a Taylor series in the reaction coordinate

$$A_k = \mu_A - \mu_B$$

$$(-A_k)_{\zeta \to 0} = \left(\frac{\partial G}{\partial \zeta}\right)_{\zeta=0} \zeta + \frac{1}{2!}\left(\frac{\partial^2 G}{\partial \zeta^2}\right)_{\zeta=0} \zeta^2 + \ldots + \frac{1}{n!}\left(\frac{\partial^n G}{\partial \zeta^n}\right)_{\zeta=0} \zeta^n$$

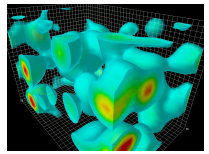

ζ is a fluctuation in a reaction coordinate, T, p, m, ξ, etc.

At equilibrium, the affinity is 0 so $\left(\frac{\partial G}{\partial \zeta}\right)_{\zeta=0} = 0$

If $\left(\frac{\partial^2 G}{\partial \zeta^2}\right)_{\zeta=0} > 0$ then the equilibrium is stable

Construction of a Phase Diagram Based on Fluctuations

Consider the Hildebrand Model

$$G_m = x_A \mu_A^o + x_B \mu_B^o + RT(x_A \ln x_A + x_B \ln x_B) + \Omega x_A x_B$$

assume that $\mu_B^o = \mu_A^o = 0$

Binodal phase equilibria is defined by

$$\frac{\partial G_m}{\partial x_B} = RT(\ln x_B - \ln x_A) + \Omega(1 - 2x_B) = 0$$

$$\ln \frac{x_B}{x_A} = -\frac{\Omega}{RT}(1 - 2x_B)$$

$x_A = 1\text{-}x_B$ and $d(\ln(x)) = dx/x$

Spinodal is defined by

$$\frac{\partial^2 G_m}{\partial x_B^2} = RT\left(\frac{1}{x_A} + \frac{1}{x_B}\right) - 2\Omega = 0 \qquad x_A x_B = (1 - x_B)x_B = \frac{RT}{2\Omega}$$

Critical Point is defined by

$d^3G_m/dx_B^3 = RT(1/(1\text{-}x_B)^2 - 1/x_B^2) = 0$ or $x_A = x_B = 0.5$

Using this composition in $d^2G_m/dx_B^2 = 0$ yields $T_c = \Omega / 2R$

Hildebrand Equation

$$G_m = x_A \mu_A^o + x_B \mu_B^o + RT(x_A \ln x_A + x_B \ln x_B) + \Omega x_A x_B \qquad \text{assume that } \mu_B^o = \mu_A^o = 0$$

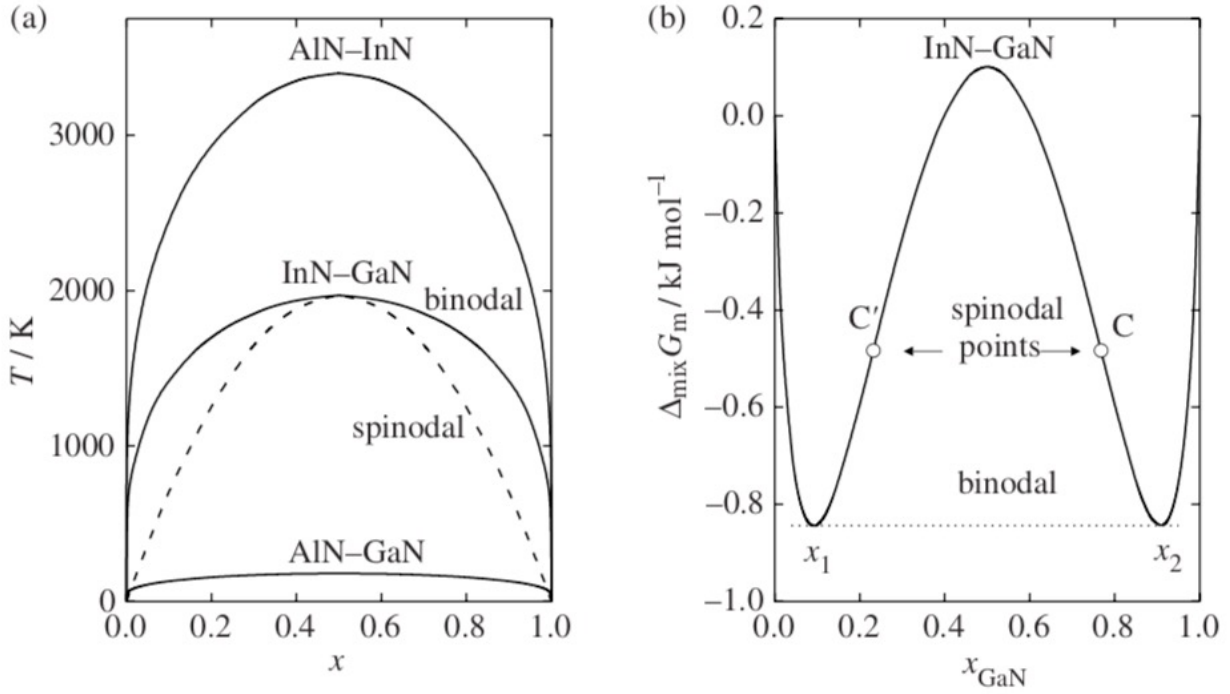

Figure 5.7 (a) Theoretical predictions of the unstable regions (miscibility gap) of the solid solutions in the systems AlN–GaN, InN–GaN and AlN–InN [15]. For the system InN–GaN both the phase boundary (binodal) and spinodal lines are shown. (b) Gibbs energy of mixing for the solid solution InN–GaN at 1400 K.

$$G_m = x_A \mu_A^o + x_B \mu_B^o + RT(x_A \ln x_A + x_B \ln x_B) + \Omega x_A x_B \qquad \text{assume that } \mu_B^o = \mu_A^o = 0$$

If Ω = -A + BT, and the entropy term is small (for polymers for instance) B is non-combinatorial entropy
Phase separation occurs on heating: Lower Critical Solution Temperature (LCST)

Flory-Huggins Equation

$$\Delta \mathcal{G}_{mix} = \tilde{R}T\tilde{n}_c \left(\frac{\phi_A}{N_A} \ln \phi_A + \frac{\phi_B}{N_B} \ln \phi_B + \chi \phi_A \phi_B \right)$$

ϕ_A is the volume fraction of A
N_A is the number of "c" units in A
n_c is the total number of c volume units in the system
C is an average of A and B units
Volume fraction has replaced mole fraction
χ is an average interaction energy per c site per RT
$\chi \sim \Omega/RT$

Symmetric blend $N_A = N_B$
Entropy part is small since $N_i \sim 100{,}000$
$\chi \sim a - b/T$ leads to LCST behavior, "a" is non-combinatorial entropy, "b" is the enthalpy of specific interactions that leads to miscibility

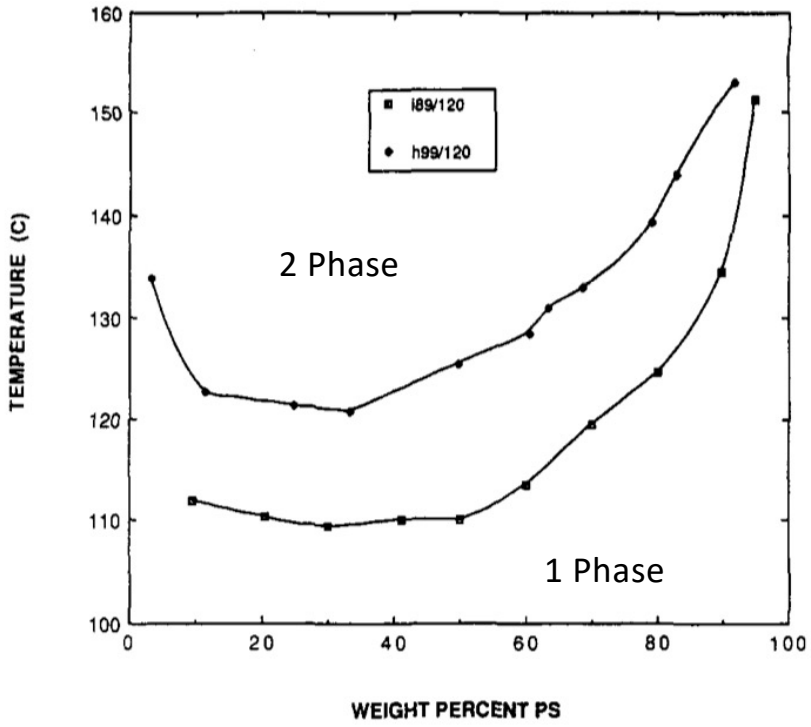

Figure 7. Cloud-point curves for i89/120 and h99/120 blends.

Since χN depends on 1/T specifying χN specifies the temperature. Large χN is low tempearature.

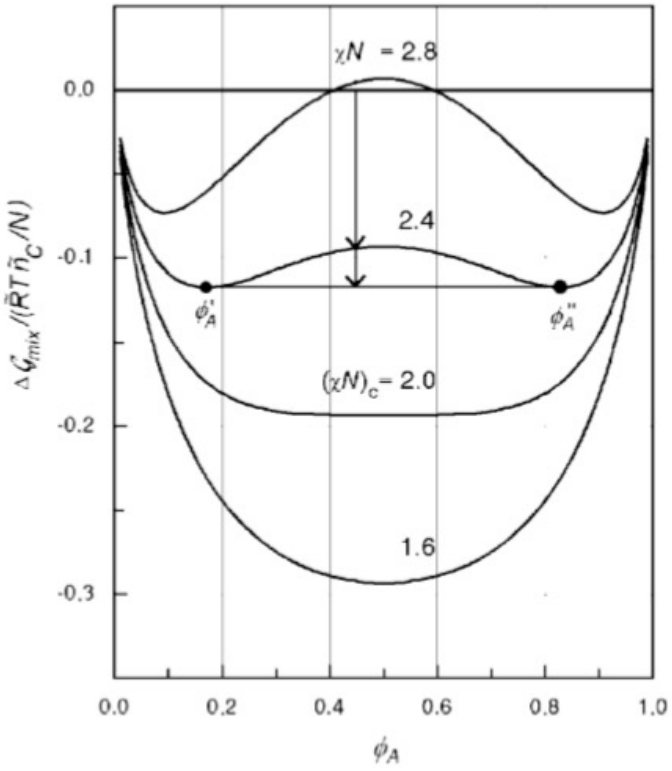

Fig. 4.3. Gibbs free energy of mixing of a symmetric binary polymer mixture ($N_A = N_B = N$), as described by the Flory–Huggins equation

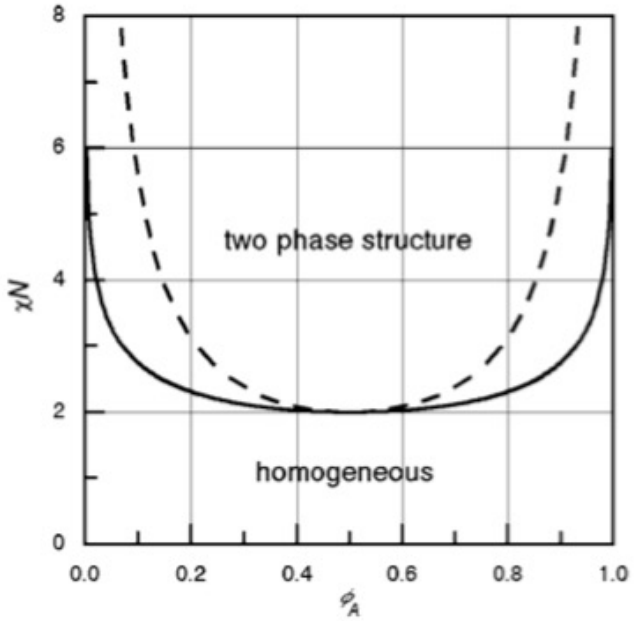

Fig. 4.4. Phase diagram of a symmetric polymer mixture ($N_A = N_B = N$). In addition to the binodal (*continuous line*) the spinodal is shown (*broken line*)

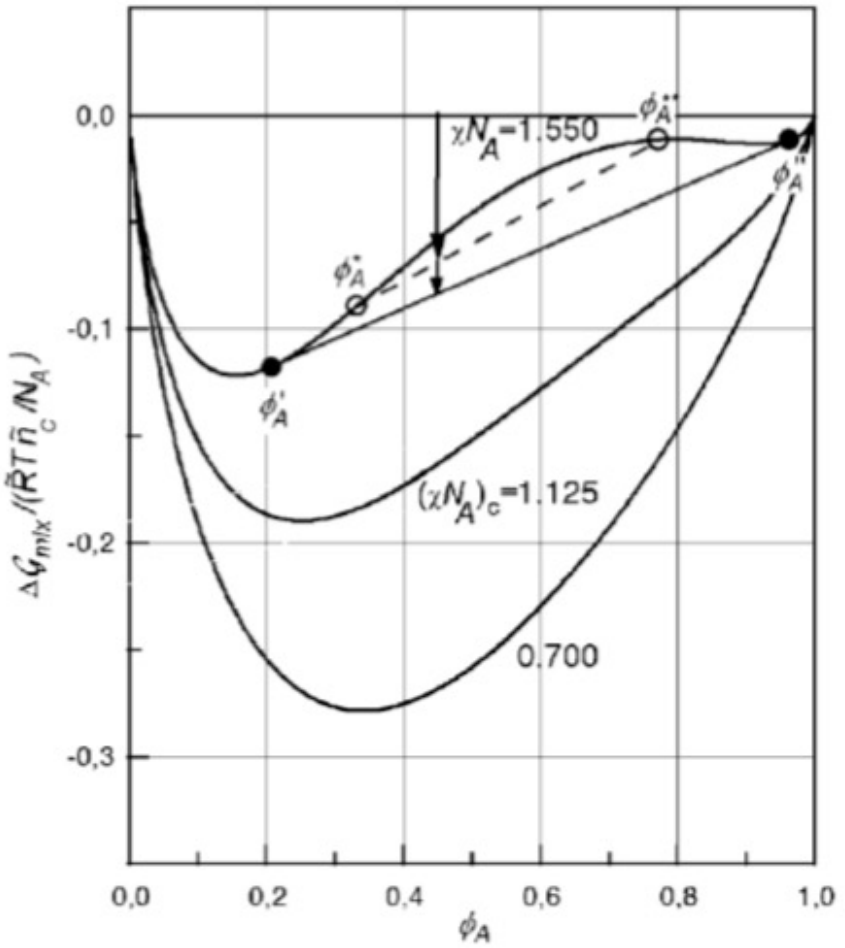

Fig. 4.5. Gibbs free energy of mixing of an asymmetric polymer mixture with $N_B = 4N_A$, calculated for the indicated values of χN_A. The points of contact with the common tangent, located at ϕ'_A and ϕ''_A, determine the compositions of the equilibrium phases on the binodal. The critical values are $(\chi N_A)_c = 9/8$ and $\phi_c = 2/3$

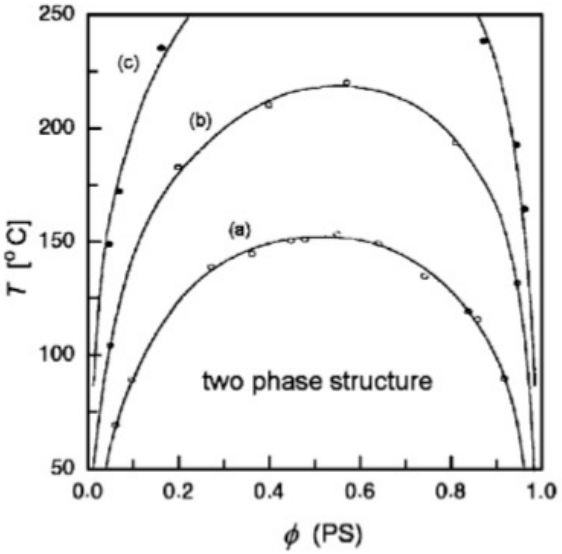

Fig. 4.8. Phase diagrams for different PS/PB-mixtures, exhibiting lower miscibility gaps. (a) $M(\mathrm{PS}) = 2250\,\mathrm{g\,mol^{-1}}$, $M(\mathrm{PB}) = 2350\,\mathrm{g\,mol^{-1}}$; (b) $M(\mathrm{PS}) = 3500\,\mathrm{g\,mol^{-1}}$, $M(\mathrm{PB}) = 2350\,\mathrm{g\,mol^{-1}}$; (c) $M(\mathrm{PS}) = 5200\,\mathrm{g\,mol^{-1}}$, $M(\mathrm{PB}) = 2350\,\mathrm{g\,mol^{-1}}$. Data from Roe and Zin [19]

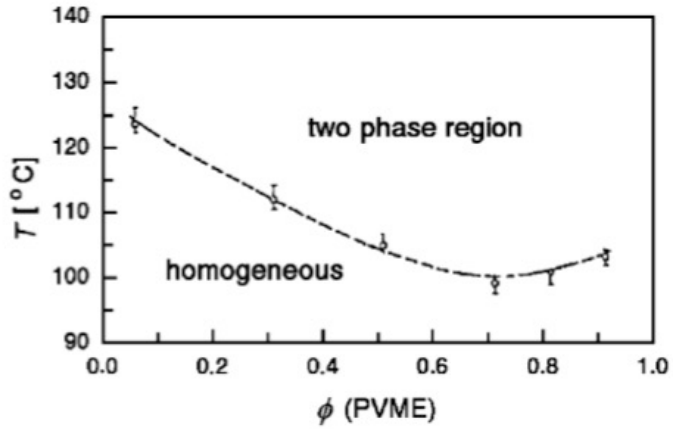

Fig. 4.9. Phase diagram of mixtures of PS ($M = 2 \times 10^5\,\mathrm{g\,mol^{-1}}$) and PVME ($M = 4.7 \times 10^4\,\mathrm{g\,mol^{-1}}$), showing an upper miscibility gap. Data from Hashimoto et al. [20]

Joon Roe

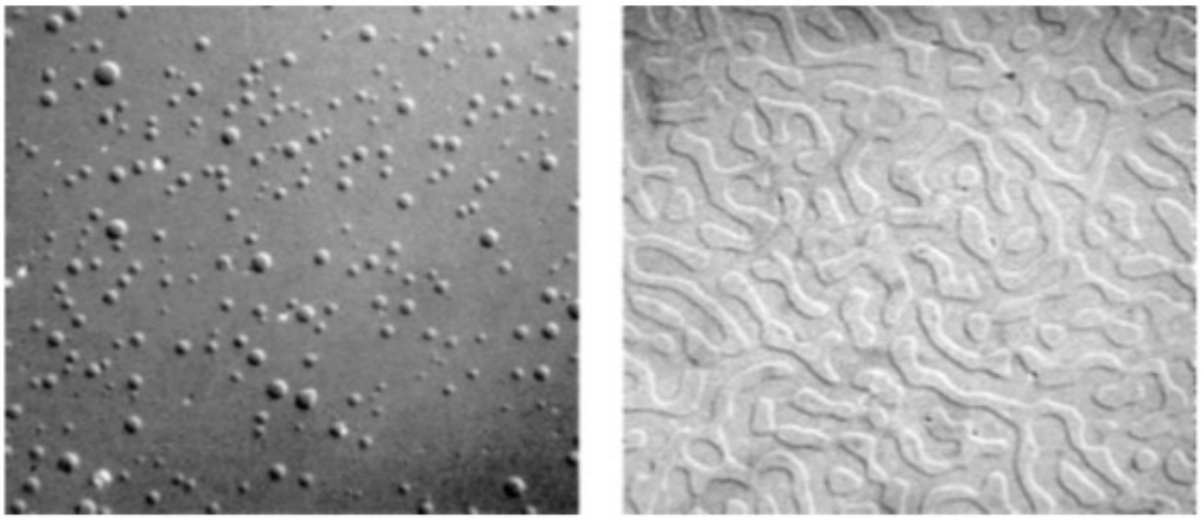

Fig. 4.10. Structure patterns emerging during phase separation in PS/PBr$_x$S-mixtures. *left*: Pattern indicating phase separation by nucleation and growth (ϕ(PS) = 0.8); *right*: Pattern suggesting phase separation by spinodal decomposition (ϕ(PS) = 0.5) [21]

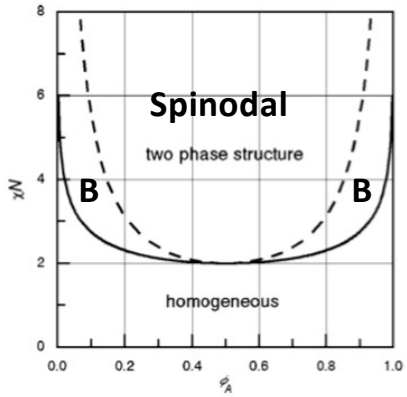

Fig. 4.4. Phase diagram of a symmetric polymer mixture ($N_A = N_B = N$). In addition to the binodal (*continuous line*) the spinodal is shown (*broken line*)

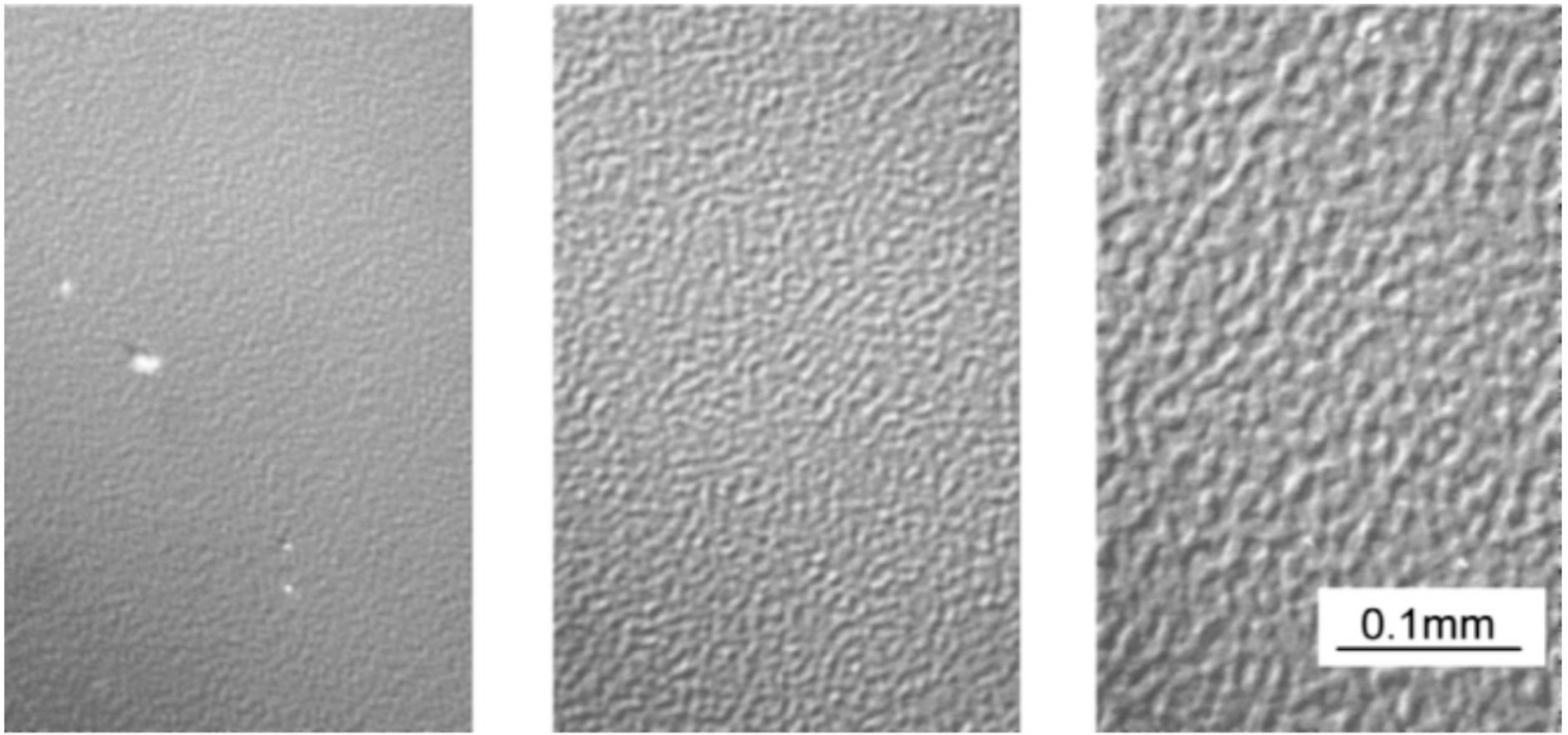

Fig. 4.24. Structure development during the late stages of spinodal decomposition observed for a PS/PBr$_x$S-(1:1) mixture. Micrographs were obtained during annealing at 200 °C ($< T_c = 220$ °C) for 1 min (*left*), 3 min (*center*) and 10 min (*right*) [21]

Iranian Polymer Journal
20 (8), 2011, 689-696

Available online at: http://journal.ippi.ac.ir

Mathematical Modelling and Phase Separation Kinetics of Polystyrene/Polyvinylmethylether Blend

Mohammad A Parsa[1], Majid Ghiass[2*], and Mohammad R Moghbeli[1]

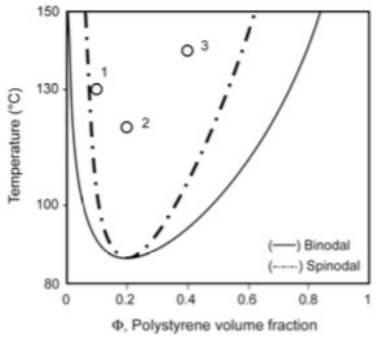

Figure 1. The phase diagram of PS/PVME blend system, three points 1, 2, and 3 are in unstable region.

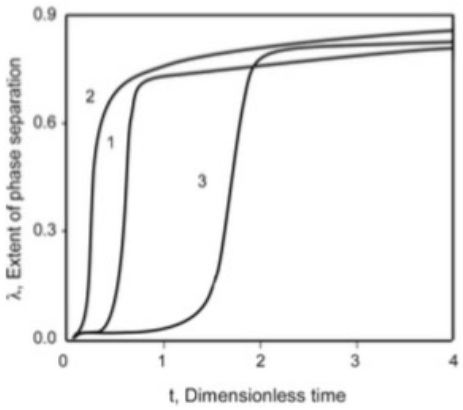

Figure 3. The extent of phase separation as a function of time for three concentration-temperature points.

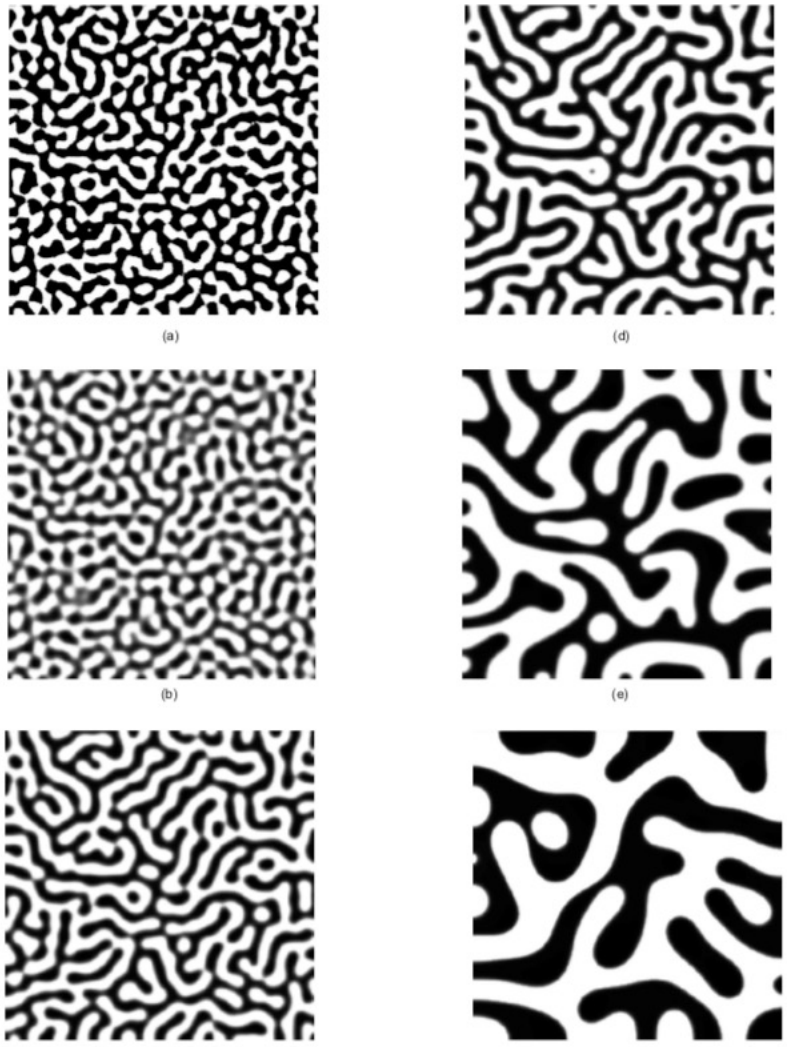

Figure 2. The dynamic morphologies of PS/PVME blend at different dimensionless times of: (a) 0.15, (b) 0.5, (c) 1, (d) 1.5, (e) 3, and (f) 7.5×10^{-3}.

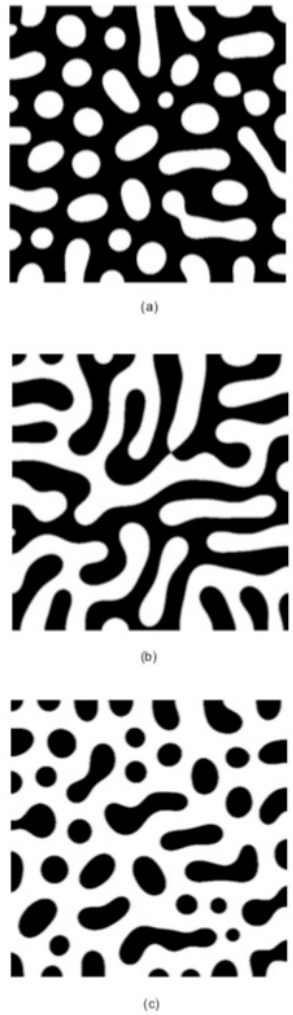

Figure 4. The final morphology of phase separated PS/PVME blend with initial concentrations of (a) 0.1, (b) 0.2, and (c) 0.4 corresponding to points 1, 2, and 3 in Figure 1.

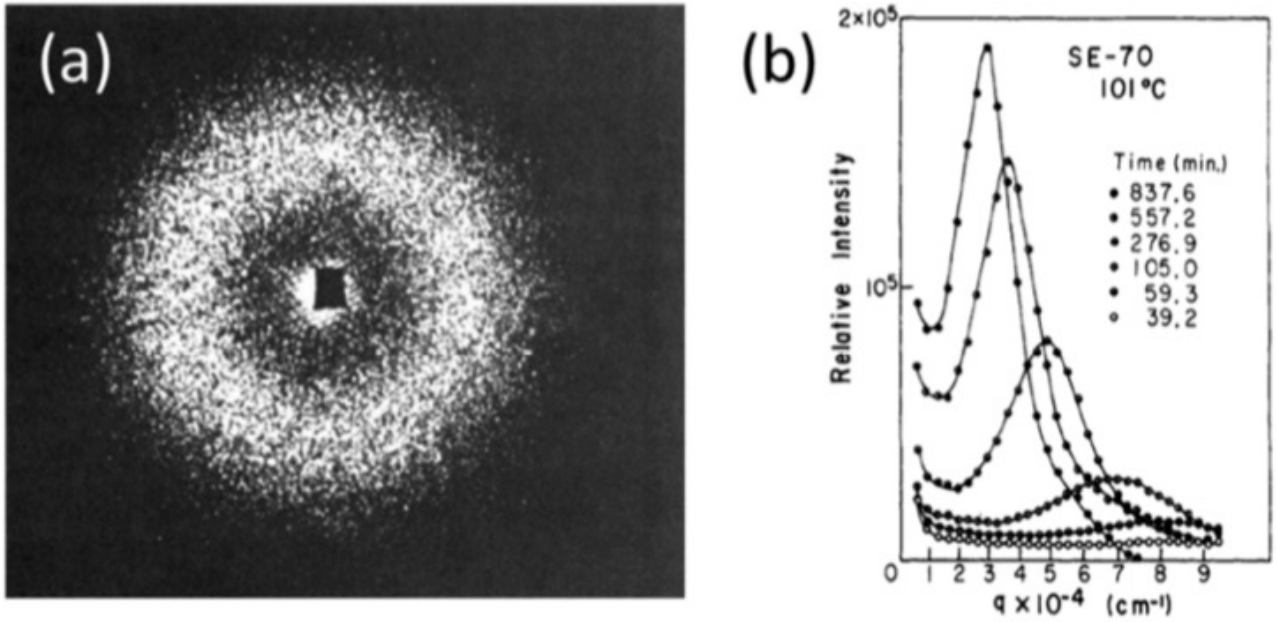

Figure 3. (a) Light scattering pattern of a demixed PS/PVME blend, reported by Snyder et al.[2] Reproduced with permission from ref 2. (b) Evolution of the (radially averaged) scattering intensity with time following the spinodal decomposition of a near-critical PS/PVME quenched ≈2 °C inside the unstable region, reported by Hashimoto et al.[3] The initial dominant length scale of the structure $\Lambda = 2\pi/q^*$, where q^* is the peak position, falls generally outside the window observed in light scattering (typically ≳300−600 nm). Reproduced with permission from ref 3.

Higgins JS, Cabral JT *A Thorny Problem? Spinodal Decomposition in Polymer Blends* Macromolecules **53** 4137−4140 (2020)

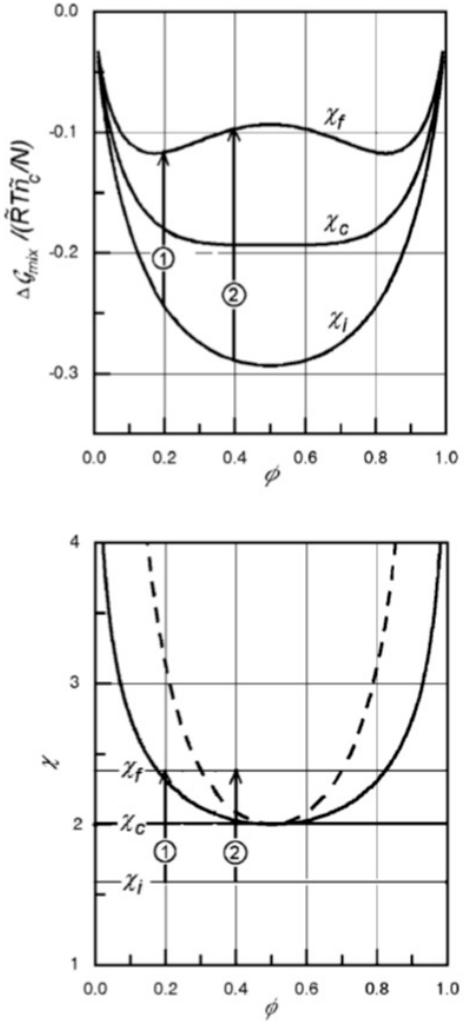

Fig. 4.11. Temperature jumps that transfer a symmetric binary polymer mixture from the homogeneous state into the two-phase region. Depending upon the location in the two-phase region, phase separation occurs either by nucleation and growth ('1') or by spinodal decomposition ('2')

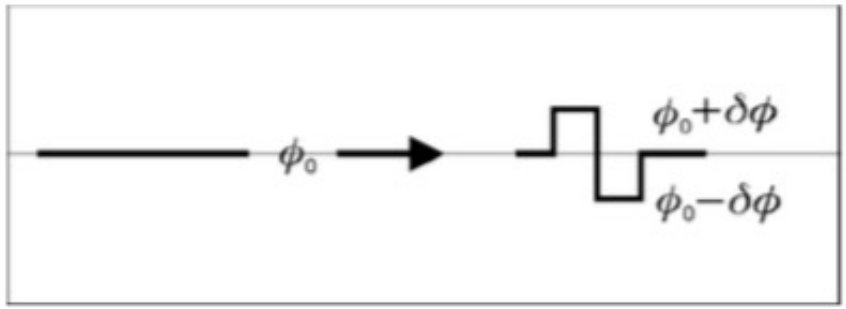

Fig. 4.12. Local concentration fluctuation

$$\delta\mathcal{G} = \frac{1}{2}(g(\phi_0 + \delta\phi) + g(\phi_0 - \delta\phi))\mathrm{d}^3\boldsymbol{r} - g(\phi_0)\mathrm{d}^3\boldsymbol{r}$$

Free energy density

Series expansion of the free energy density yields,

$$\delta\mathcal{G} = \frac{1}{2}\frac{\partial^2 g}{\partial\phi^2}(\phi_0)\delta\phi^2\mathrm{d}^3\boldsymbol{r}$$

Positive second derivative leads to increase (Stable)
(Smile up)

Negative to decrease (Phase Separation)
(Frown down)

P. 125 Strobl Chapter 4

Diffusion in Nucleation and Growth and in Spinodal Decomposition

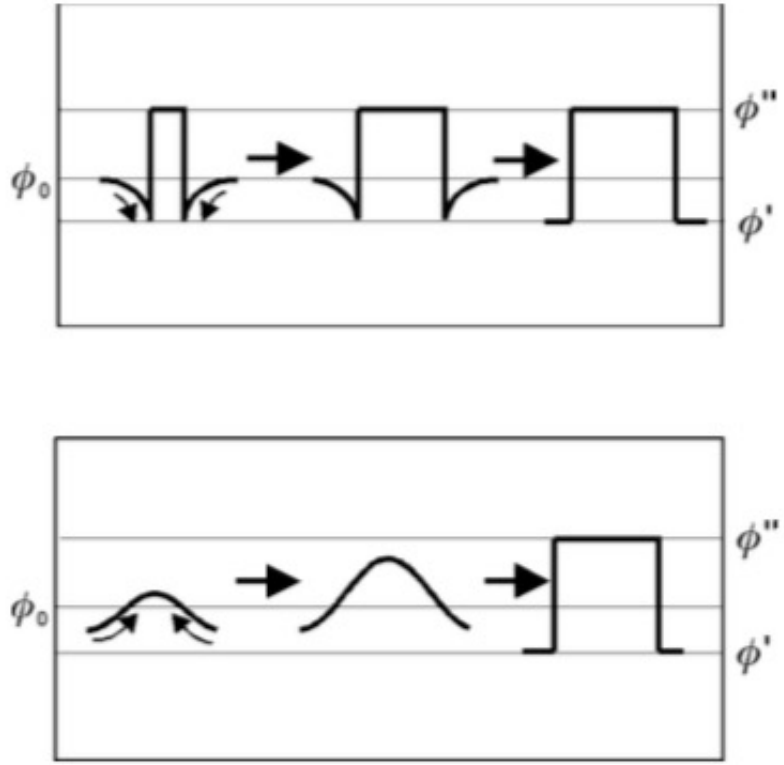

Fickian diffusion down a concentration gradient

Spinodal diffusion up a concentration gradient driven by free energy

Fig. 4.13. Mechanisms of phase separation: Nucleation and growth (*top*) and spinodal decomposition (*bottom*). The *curved small arrows* indicate the direction of the diffusive motion of the A-chains

Diffusion in Nucleation and Growth

P. 127 Strobl Chapter 4

$\Delta\mathcal{G}$ depends on the radius r of the precipitate, as described by the equation

$$\Delta\mathcal{G}(r) = -\frac{4\pi}{3} r^3 \Delta g + 4\pi r^2 \sigma_{\mathrm{if}} \qquad (4.49)$$

with

$$\Delta g = g(\phi_0) - g(\phi'') \; . \qquad (4.50)$$

Rate of Nucleation

$$\nu_{\mathrm{nuc}} \propto \exp - \frac{\Delta\mathcal{G}_{\mathrm{b}}}{kT} \; , \qquad (4.51)$$

Free energy Barrier

$$\Delta\mathcal{G}_{\mathrm{b}} = \frac{16\pi}{3} \frac{\sigma_{\mathrm{if}}^3}{(\Delta g)^2} \; . \qquad (4.52)$$

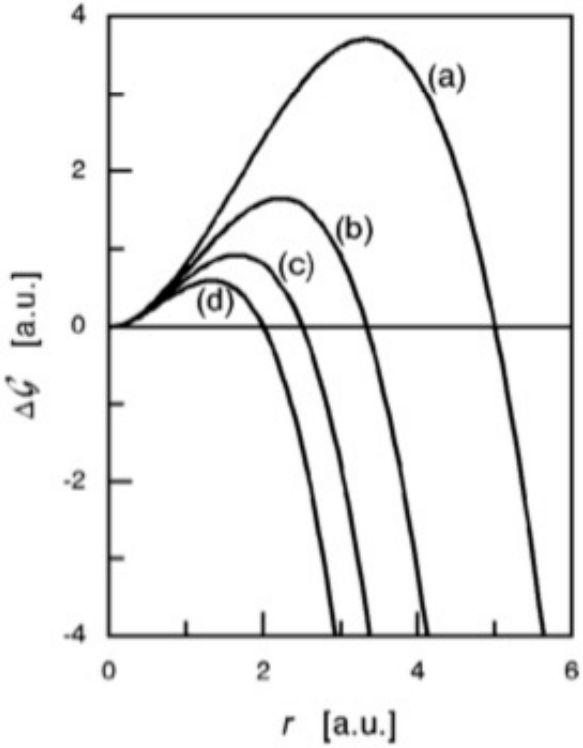

Fig. 4.14. Activation barrier encountered during formation of a spherical nucleus. Curves (a)–(d) correspond to a sequence 2:3:4:5 of values for $\Delta g/\sigma_{\mathrm{if}}$

Phase grows from fluctuations

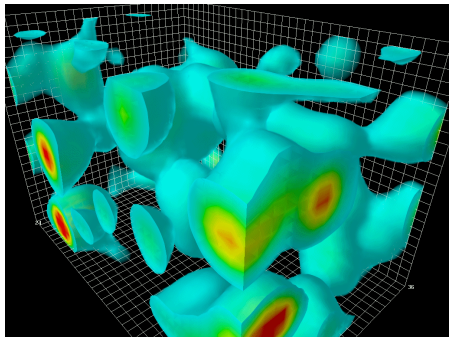

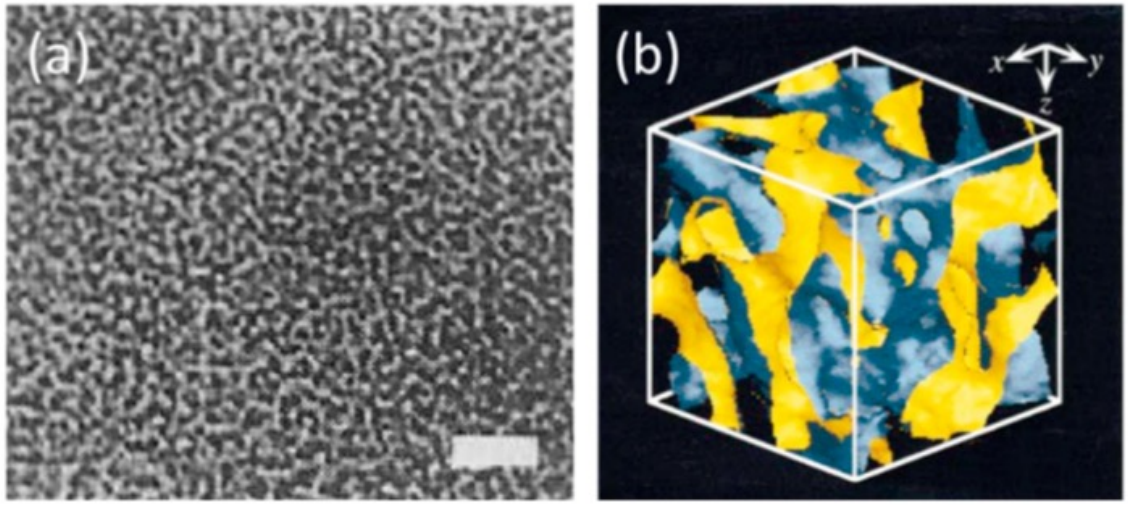

Figure 1. (a) Optical microscopy image of a demixed PS/PVME blend, of near-critical composition quenched into the unstable region (105 °C) after 300 s, reported by Nishi et al.;[1] the scale bar indicates 10 μm. Reproduced with permission from ref 1. (b) 3D image obtained by stacking of laser scanning confocal microscopy (LSCM) scans of a late-stage spinodal structure of a polybutadiene/poly(styrene-*ran*-butadiene), after Jinnai et al.;[7] the box size is 30 × 30 × 30 μm^3. Reproduced with permission from ref 7. Copyright 1997 American Physical Society.

Higgins JS, Cabral JT *A Thorny Problem? Spinodal Decomposition in Polymer Blends* Macromolecules **53** 4137−4140 (2020)

Macromolecules 1983, *16*, 641–648

Time-Resolved Light Scattering Studies on Kinetics of Phase Separation and Phase Dissolution of Polymer Blends.† 1. Kinetics of Phase Separation of a Binary Mixture of Polystyrene and Poly(vinyl methyl ether)

Takeji Hashimoto,* Jiro Kumaki,‡ and Hiromichi Kawai

Department of Polymer Chemistry, Faculty of Engineering, Kyoto University, Kyoto 606, Japan. *Received June 2, 1982*

$$F = \int dv\, [f(c) + \kappa(\nabla c)^2 + \ldots]$$

where $f(c)$ is free energy density of the system having composition c of one component (e.g., A) which is uniform everywhere in space and the second term is the excess free energy arising from a concentration gradient. The quantity c refers to volume fraction of one of the components. By taking the variational derivative of eq II-1, one obtains ($\mu_A - \mu_B$), the chemical potential difference. The flux of each component (J_A or J_B) is then obtained from $D_c(\mu_A - \mu_B)$. An application of the continuity equation $\partial c/\partial t = -\text{div}\, J_A$ to J_A results in the diffusion equation given by

$$\partial c/\partial t = D_c(\partial^2 f/\partial c^2)\nabla^2 c - 2D_c\kappa\nabla^4 c + \ldots$$

The solution of eq II-2 is obtained by

$$c(\mathbf{r}) - c_0 = \sum_{\mathbf{q}} \exp[R(\mathbf{q})t]\{A(\mathbf{q}) \cos(\mathbf{q}\cdot\mathbf{r}) + B(\mathbf{q}) \sin(\mathbf{q}\cdot\mathbf{r})\}$$

Growth rate at q

$$R(q) = D_c q^2\{-(\partial^2 f/\partial c^2) - 2\kappa q^2\} \qquad \text{(II-4)}$$

where $q = 2\pi/\Lambda$ is the wavenumber of the spatial composition fluctuations and Λ is the corresponding wavelength. The fluctuation $\Delta c(\mathbf{r}) = c(\mathbf{r}) - c_0$ is assumed to be

Macromolecules 1983, *16*, 641–648

Time-Resolved Light Scattering Studies on Kinetics of Phase Separation and Phase Dissolution of Polymer Blends.† 1. Kinetics of Phase Separation of a Binary Mixture of Polystyrene and Poly(vinyl methyl ether)

Takeji Hashimoto,* Jiro Kumaki,‡ and Hiromichi Kawai

Department of Polymer Chemistry, Faculty of Engineering, Kyoto University, Kyoto 606, Japan. *Received June 2, 1982*

$$\tilde{F}/k_B T = (1/N)[c \ln c + (1-c) \ln (1-c)] + \chi c(1-c) + [a^2/(36c(1-c))](\nabla c)^2 + \ldots$$

Flory-Huggins with a gradient term

Macromolecules 1983, *16*, 641–648

Time-Resolved Light Scattering Studies on Kinetics of Phase Separation and Phase Dissolution of Polymer Blends.† 1. Kinetics of Phase Separation of a Binary Mixture of Polystyrene and Poly(vinyl methyl ether)

Takeji Hashimoto,* Jiro Kumaki,‡ and Hiromichi Kawai

Department of Polymer Chemistry, Faculty of Engineering, Kyoto University, Kyoto 606, Japan. *Received June 2, 1982*

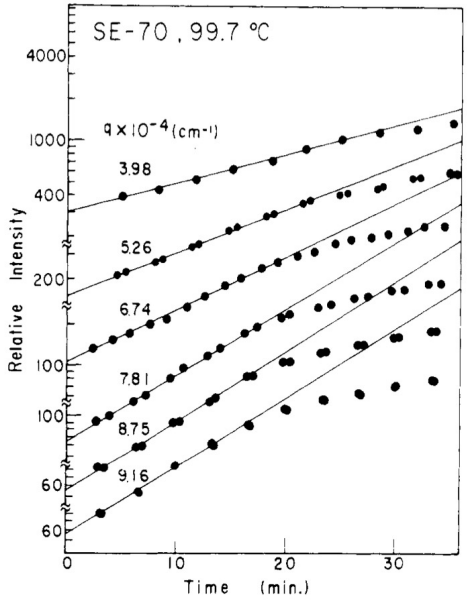

$$I(q, t) \sim \mathcal{F}\{\Delta\tilde{c}^2(\mathbf{r})\} = I(q, t = 0) \exp[2R(q)t]$$

R(q) can be measured by light scattering
For Polymers
(X-ray or neutron for metals/ceramics)

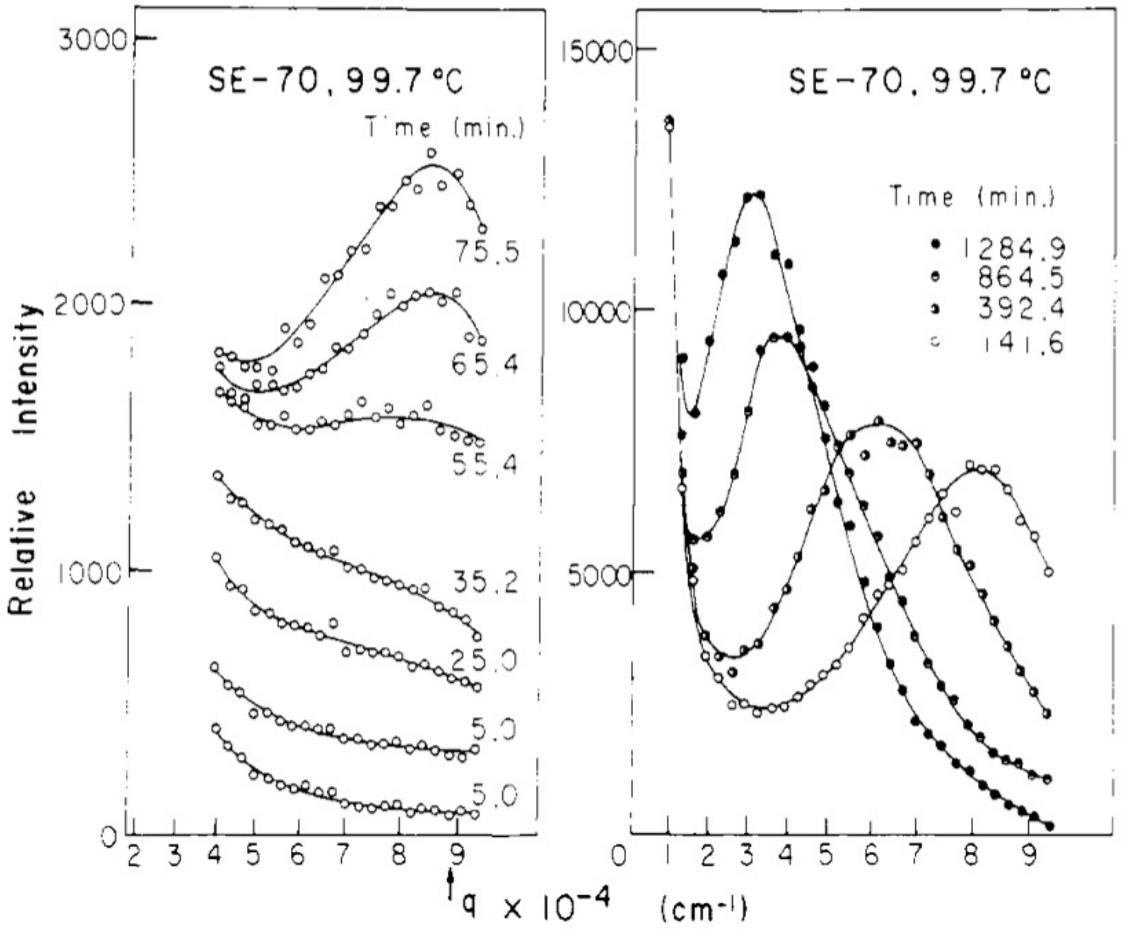

Figure 3. Change of the scattered intensity profiles with time during a course of SD of the polymer blend SE-70 at T_x = 99.7 °C. $q = (4\pi/\lambda) \sin(\theta/2)$. The superheating from the spinodal point T_s, $\Delta T = |T_x - T_s|$ = 0.5 °C.

Macromolecules 1983, *16*, 641–648

Time-Resolved Light Scattering Studies on Kinetics of Phase Separation and Phase Dissolution of Polymer Blends.† 1. Kinetics of Phase Separation of a Binary Mixture of Polystyrene and Poly(vinyl methyl ether)

Takeji Hashimoto,* Jiro Kumaki,‡ and Hiromichi Kawai

Department of Polymer Chemistry, Faculty of Engineering, Kyoto University, Kyoto 606, Japan. *Received June 2, 1982*

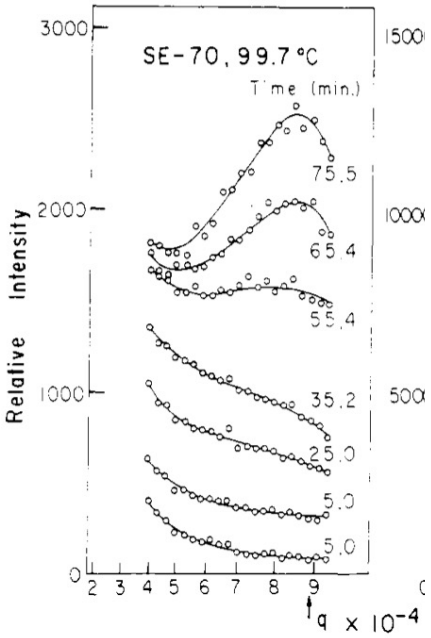

$$q_m^2 = q_c^2/2 = -(\partial^2 f/\partial c^2)/4\kappa \qquad \text{(II-7)}$$

$$R(q_m) = -D_c(\partial^2 f/\partial c^2)/8\kappa \qquad \text{(II-8)}$$

It should be noted that q_m is controlled only by *thermodynamics* while $R(q_m)$ is controlled also by the *transport property* D_c. At the spinodal point $T = T_s$,

$$R(q) = q^2 D_c\left[\left(\frac{\chi - \chi_s}{\chi_s}\right) - \left(\frac{R_0^2}{36}\right)q^2\right]$$

Transport Thermodynamics Size (Entropy of the gradient)

$$-\frac{\partial^2 f}{\partial c^2} = \frac{\chi - \chi_s}{\chi_s} \qquad \kappa = R_0^2/72$$

Macromolecules 1983, *16*, 641–648

Time-Resolved Light Scattering Studies on Kinetics of Phase Separation and Phase Dissolution of Polymer Blends.† 1. Kinetics of Phase Separation of a Binary Mixture of Polystyrene and Poly(vinyl methyl ether)

Takeji Hashimoto,* Jiro Kumaki,‡ and Hiromichi Kawai

Department of Polymer Chemistry, Faculty of Engineering, Kyoto University, Kyoto 606, Japan. *Received June 2, 1982*

Activation Barrier for Nucleation and Growth

Different relative bulk to surface free energies (small to large)

Rate of Nucleation

$$\nu_{\text{nuc}} \propto \exp - \frac{\Delta \mathcal{G}_{\text{b}}}{kT}$$

Free energy Barrier

$$\Delta \mathcal{G}_{\text{b}} = \frac{16\pi}{3} \frac{\sigma_{\text{if}}^3}{(\Delta g)^2}$$

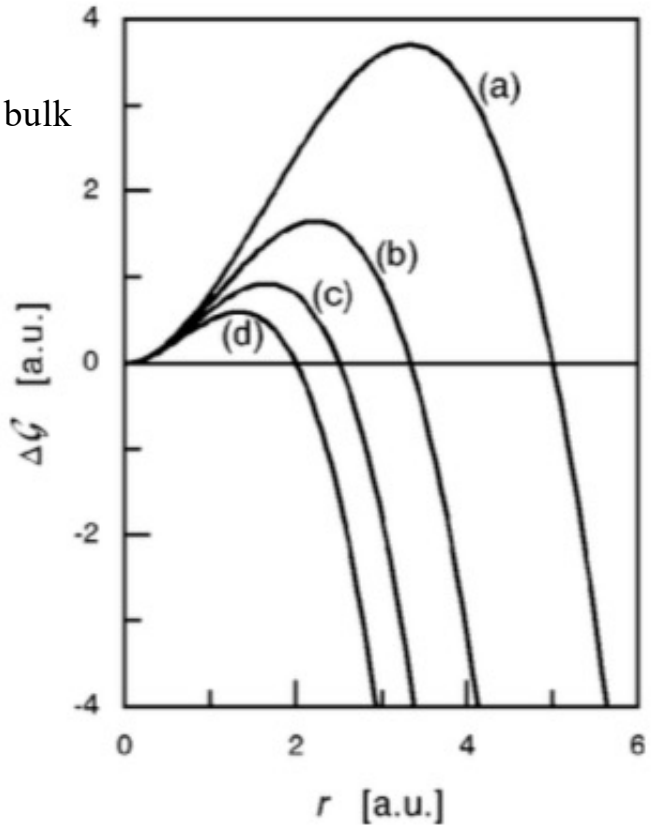

$$\Delta \mathcal{G}(r) = -\frac{4\pi}{3} r^3 \Delta g + 4\pi r^2 \sigma_{\text{if}}$$

$$\Delta g = g(\phi_0) - g(\phi'') \ .$$

Balance between bulk and surface Free energies
(Next chapter)

Fig. 4.14. Activation barrier encountered during formation of a spherical nucleus. Curves (a)–(d) correspond to a sequence 2:3:4:5 of values for $\Delta g/\sigma_{\text{if}}$

Critical Scattering from Single Phase Polymer Melt (neutron scattering 10Å)

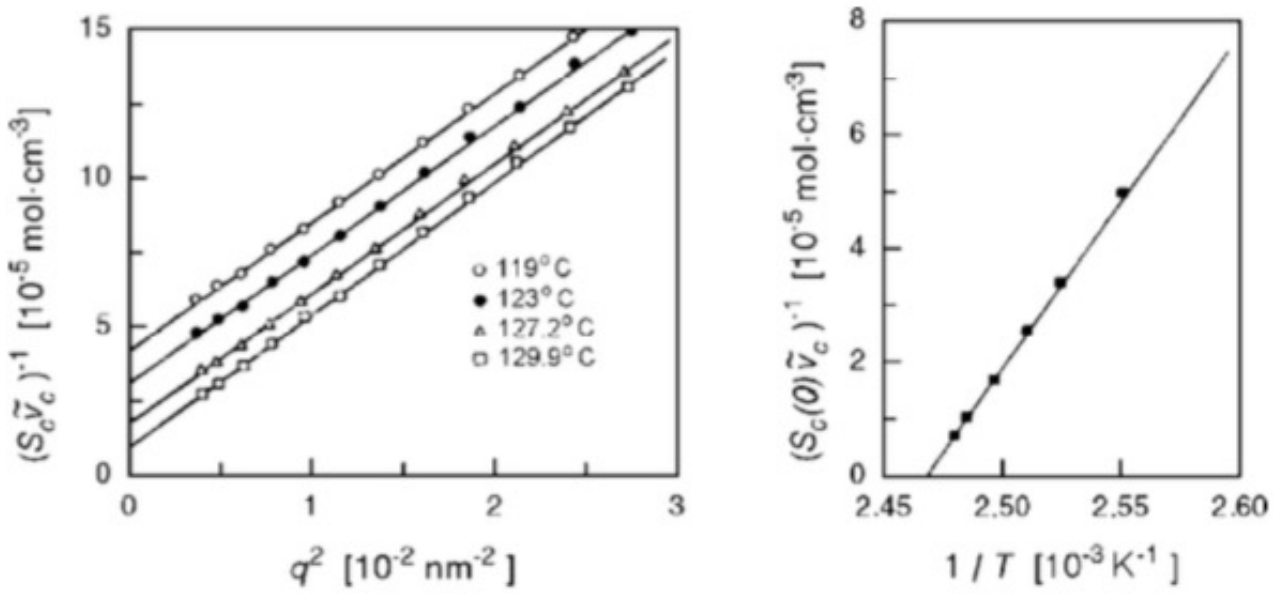

Fig. 4.15. Results of neutron scattering experiments on a (0.13:0.87)-mixture of d-PS ($M = 3.8 \times 10^5\,\mathrm{g\,mol^{-1}}$) and PVME ($M = 6.4 \times 10^4\,\mathrm{g\,mol^{-1}}$). S_c denotes the scattering function Eq. (4.79) referring to structure units with a molar volume $\tilde{v}_c$. Intensities increase on approaching the critical point (*left*). Extrapolation of $S(q \to 0)$ to the point of divergence yields the critical temperature (*right*). Data from Schwahn et al. [22]

A polymer chain in a melt is a random walk like a diffusion path so Mass ~ size^2

By Bragg's law size is related to inverse angle

$d = 2/(\lambda \sin\theta)$

Reduced angle is $q = 4\pi/\lambda \sin\theta$

Intensity (S) scales with Mass

So, $S \sim q^{-2}$

Then a plot of 1/S vs q^2 should be a line that reflects the inverse of contrast at q = 0

At the critical point contrast goes to ∞ so 1/S goes to 0.

Deuteration provides contrast for neutrons, λ = 10Å.

After a T-jump to the 2-Phase region (Light Scattering 0.6 µm)

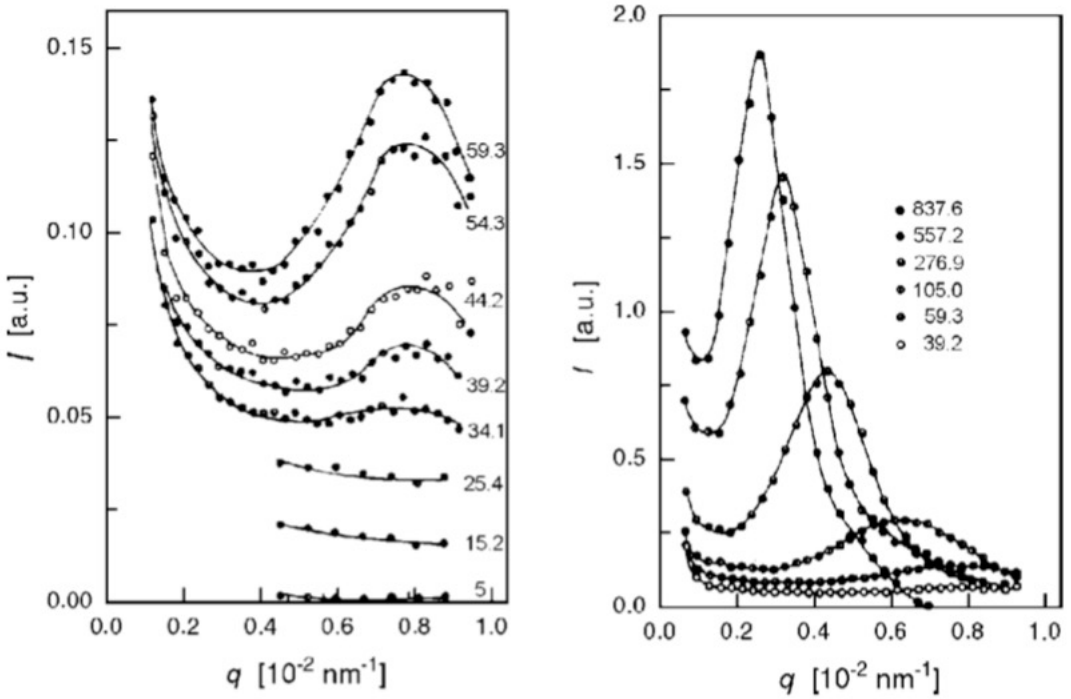

Fig. 4.17. Time dependent light scattering experiments, conducted on a (0.3:0.7)-mixture of PS ($M = 1.5 \times 10^5\,\mathrm{g\,mol^{-1}}$) and PVME ($M = 4.6 \times 10^4\,\mathrm{g\,mol^{-1}}$) subsequent to a rapid transfer from a temperature in the region of homogeneous states to the temperature $T_{\mathrm{fi}} = 101\,^{\circ}\mathrm{C}$ located in the two-phase region. Numbers give the time passed after the jump (in seconds). Data from Hashimoto et al. [23]

Vycor and Pyrex Glass
$Na_2B_8O_{13}$-SiO_2

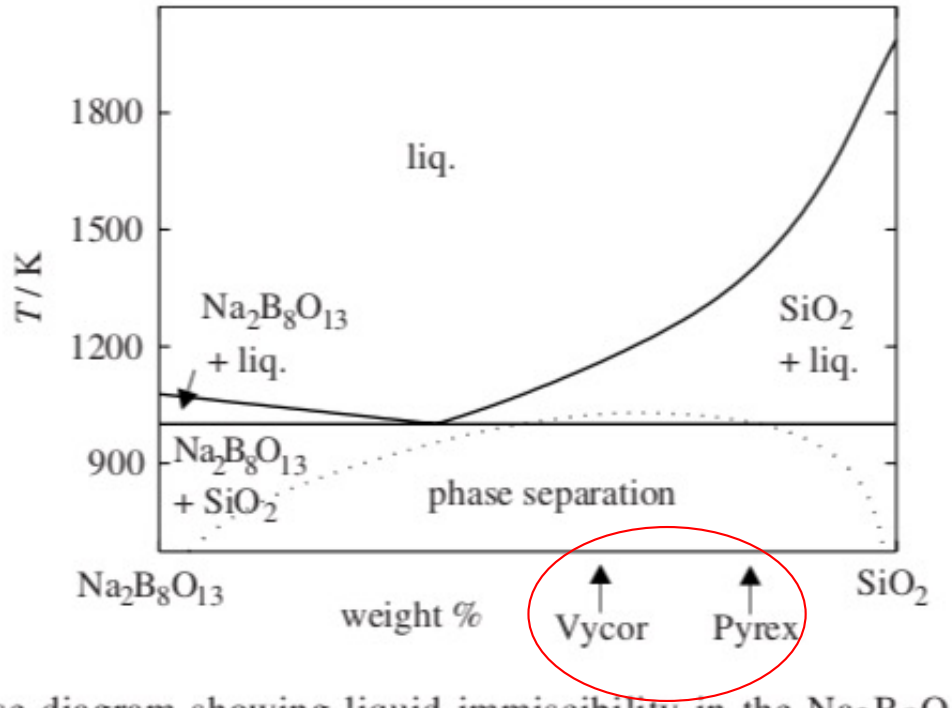

Figure 5.9 Phase diagram showing liquid immiscibility in the $Na_2B_8O_{13}$–SiO_2 system below the liquidus [16].

Vycor

Pure fused silica is difficult to shape
Adding boron trioxide makes the melt more formable
Phase separation in the **spinodal** region leads to **continuous phases**
The boron can be leached out using acid leading to 96% silica in a simple process
Pure fused silica is very strong and resists thermal shock due to low thermal expansion coefficient (High precision lenses)
If the glass is not reheated to remove the pores it can be used as a filter or water absorber

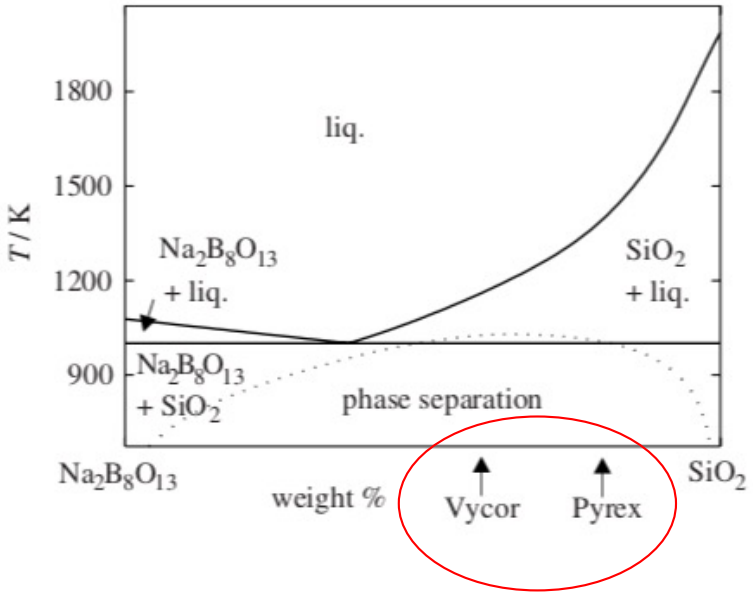

Pyrex

Adding boron trioxide makes the melt more formable and have a lower thermal expansion coefficient (1911).
Phase separation in the **binodal** region leads to boron domains in a silica matrix. This composition is used for Corelleware™
2-phase white translucent ceramic

$(dP/dV)_T = -(dT/dV)_P\,(dP/dT)_V$ Triple Product Rule

$= -(1/\alpha)(\alpha/\kappa)$ First by def. second from Cp Cv calc.

$= -1/\kappa$

So, the P vs. V plot must have a negative slope!!

Positive slope part is imaginary

In the miscible region, changes in V occur by converting liquid to solid or solid to liquid at constant P so $(dP/dV)_T = 0$ in the 2-phase region.

van der Waals Equation
(isothermal plot)

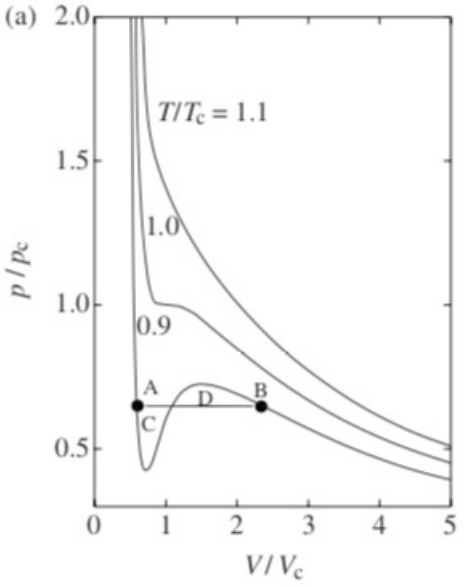

Van der Waals

$$P = \frac{RT}{V-b} - \frac{a}{V^2}$$

$$\left(\frac{\partial p}{\partial V}\right)_{T_c} = \left(\frac{\partial^2 p}{\partial V^2}\right)_{T_c} = 0$$

At T_c, P_c

$$a = \frac{27}{64}\frac{(RT_c)^2}{P_c} \qquad b = \frac{RT_c}{8P_c}$$

$$\left(\bar{p} + \frac{3}{\bar{V}^2}\right)(3\bar{V} - 1) = 8\bar{T}$$

At the critical point
$T/T_c = 1$ $(\partial^2 G/\partial p^2)_T = 0, (\partial^3 G/\partial p^3)_T = 0.$

P ~ 1/V ideal gas

$$\bar{p} = p/p_c, \bar{T} = T/T_c \text{ and } \bar{V} = V/V_c$$

$$A(V) = -\int_{V_i}^{V_f} p\,dV$$

$(\partial p / \partial V)_T = 0$
In two phase region

$(\partial p/\partial V)_T < 0$
Is unphysical
Negative
compressibility

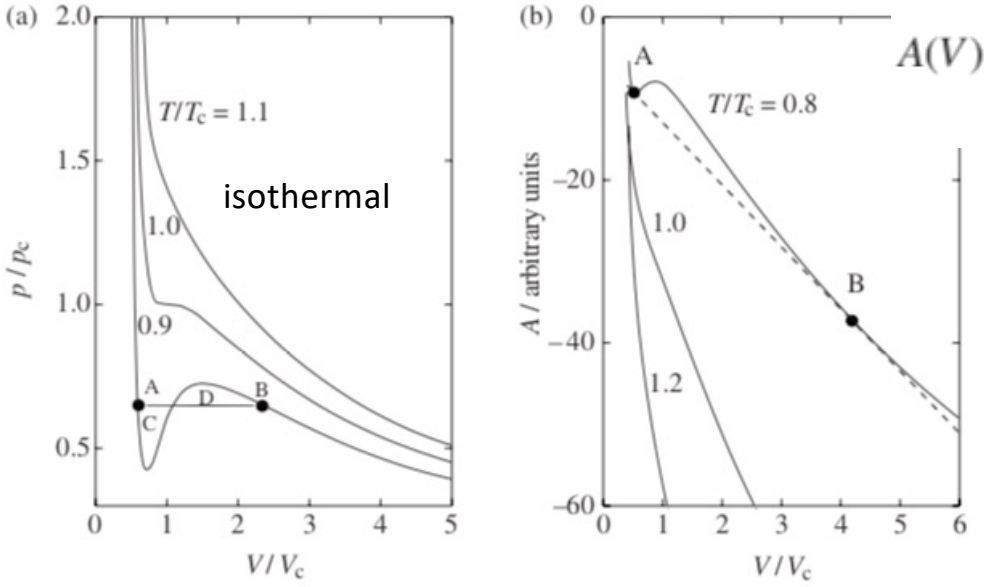

Common Tangent Method for $T/T_c = 0.8$

Maxwell equal area construction

Figure 5.10 (a) p-V isotherms of the van der Waals equation of state for H_2O at $T/T_c = 1.1$, 1.0 and 0.9. (b) The Helmholz energy $A(T,V)$ for the van der Waals equation of state of H_2O as a function of V/V_c at $T/T_c = 1.2$, 1.0 and 0.8.

P ~ T ideal gas

isochoric

isobaric

Vapor pressure of water

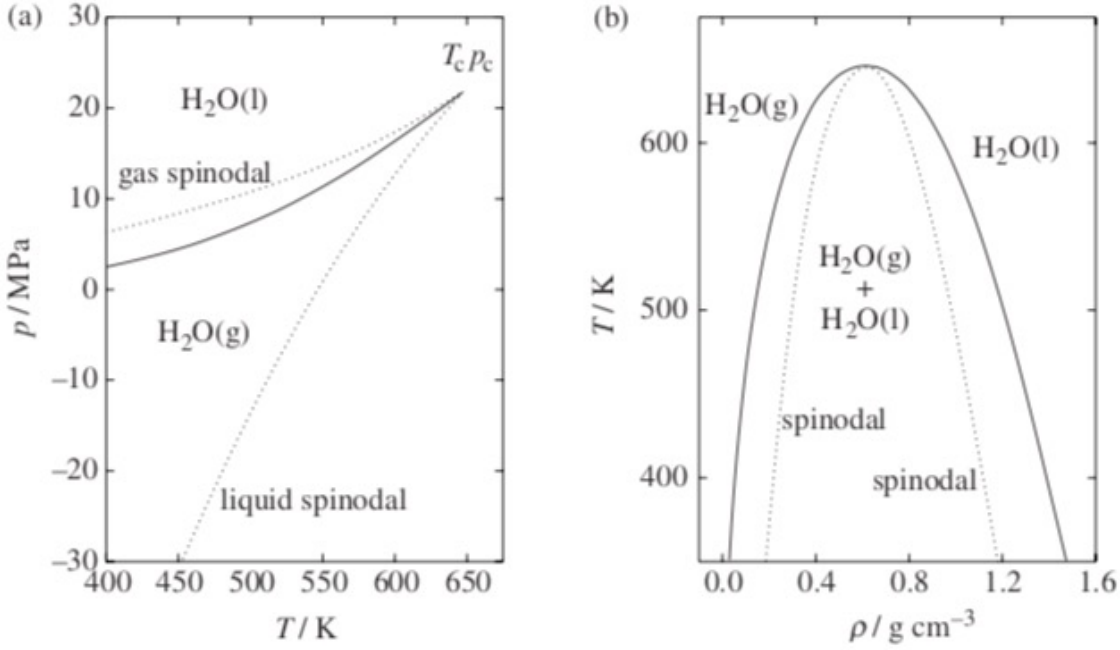

Figure 5.11 The p-T (a) and the T-ρ (b) phase diagrams of H_2O calculated using the van der Waals equation of state.

Polymorphs and Allotrophs

Allotroph ***of a single element***: Carbon as diamond or graphite

Polymorph ***of a compound***:

Titania as anatase or rutile

Silica as α-quartz, β-quartz, tridymite, cristobalite, moganite, coesite, and stishovite

Calcium carbonate as calcite or argonite

Calcite (on left) and Aragonite (on right). Both crystals are made out of calcium carbonate, making these crystals dimorphic.

Ostwald's rule: Most stable polymorph does not always crystallize, rather, meta-stable polymorphs form at a higher rate if the surface tension difference between the melt/liquid solution and the polylmorph is small.

Ostwald ripening: Metastable polymorphs may form small crystals. Over time stable polymorphs grow from these small crystals into large crystals. This has been generalized to growth of large phases due to ripening such as in crushed ice or ice cream.

Ostwald-Freundlich Equation: Small crystals dissolve more easily than large crystals. This is the reason for Ostwald ripening. Also true for vapor pressure of a liquid droplet (replace x with p)

$$\frac{p}{p_{\text{eq}}} = \exp\left(\frac{R_{\text{critical}}}{R}\right)$$

$$R_{critical} = \frac{2 \cdot \gamma \cdot V_{\text{atom}}}{k_{\text{B}} \cdot T}$$

V_{atom} = atomic volume

k_{B} = Boltzmann constant

γ = surface tension ($\text{J} \cdot \text{m}^{-2}$)

p_{eq} = equilibrium partial pressure (or chemical potential or concentration)

p = partial pressure (or chemical potential or concentration)

T = absolute temperature

Ostwald step rule: Least stable polymorph crystallizes first since it has a free energy that is closest to the liquid or solution state. This means that metastable phases form kinetically first if they exist. If many polymorphs exist, they will form in order of free energy with the highest forming first.

During the course of his academic career, Ostwald published more than 500 original research papers for the scientific literature and approximately 45 books.[9]

Real-Time Observation of $CaCO_3$ Mineralization in Highly Supersaturated Graphene Liquid Cells

Kyun Seong Dae, Joon Ha Chang, Kunmo Koo, Jungjae Park, Jae Sung Kim, and Jong Min Yuk*

ACS Omega 2020, 5, 14619−14624

1 Nucleation, 2 diffusion-limited growth, and 3 Ostwald ripening/coalescence.

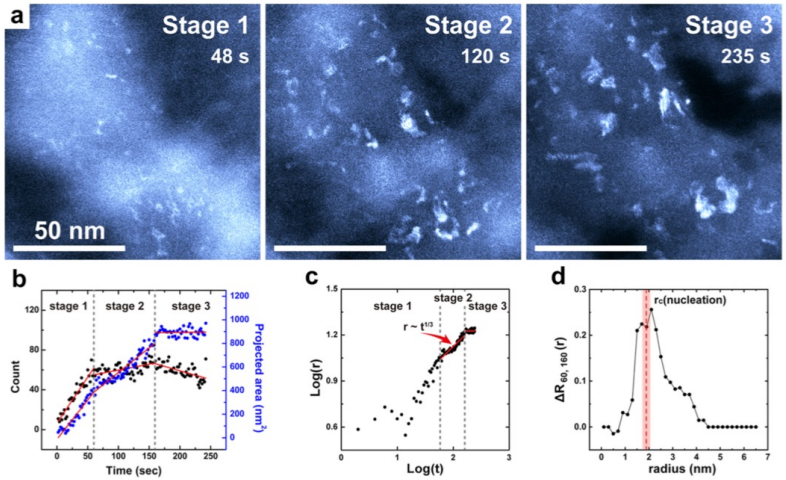

Figure 2. *In situ* dark-field TEM analysis of $CaCO_3$ crystallization. (a) Time series images corresponding to each mineralization stage. (b) Each black and blue dot gives the number of particles and total projected area of all precipitates as a function of irradiation time *t*. Based on the dynamics of mineralization, the whole process is divided into three stages: nucleation, diffusion-limited growth, and Ostwald ripening/coalescence. Red solid lines show the trends in each stage. (c) Logarithm relationship between the radius *r* of the particles and *t*. (d) Increase in the ratio of the number of particles larger than *r* during the growth step (Stage 2), $\Delta R_{60,160}(r)$. The peak indicated by the red dotted line shows the critical radius for the nucleation, r_c(nucleation).

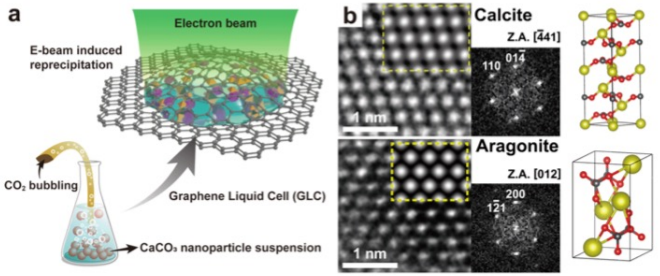

Figure 1. (a) Schematic of the GLC structure containing the calcium bicarbonate solution. The precursor solution is prepared by bubbling carbon dioxide gas into the calcite-suspended water. The precursor solution is then trapped with multilayer graphene membranes. When the GLC was exposed to the electron beam, particles are precipitated as water evaporates. (b) Filtered HRTEM images of the precipitates and the corresponding FFTs with each crystal structure of calcite and aragonite. Simulated images are presented in each of the HRTEM images, surrounded by the dotted yellow line. Z.A. is the zone axis.

Crystallization behavior of amorphous $BaTiO_3$ thin films

J Mater Sci (2020) 55:8793–8801

Gyung Hyun Ryu[1], Neal P. Lewis[1], George N. Kotsonis[1,2], Jon-Paul Maria[1,2], and Elizabeth C. Dickey[1,*]

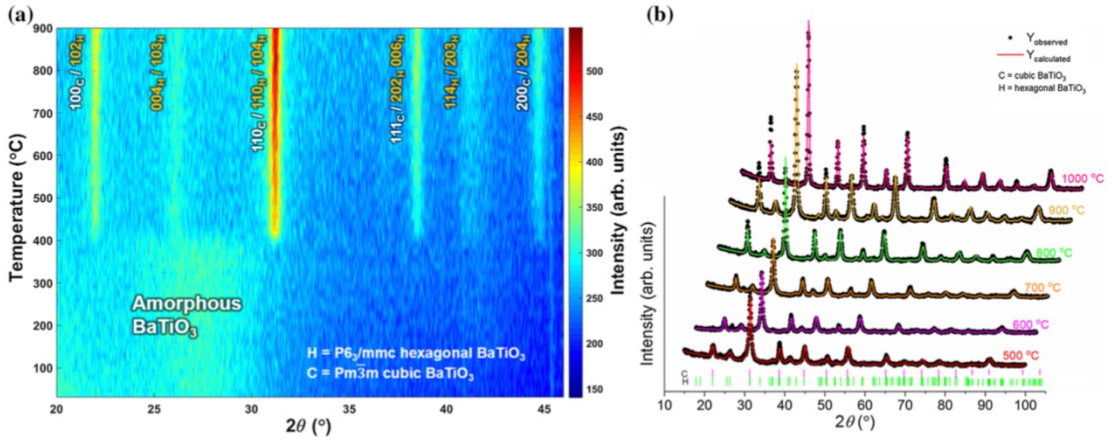

Figure 1 **a** In situ high-temperature X-ray diffraction patterns of amorphous $BaTiO_3$ film on c-sapphire. **b** Observed and fitted room-temperature GIXRD patterns of $BaTiO_3$ film isothermally annealed from 500 to 1000 °C for 2 h in air.

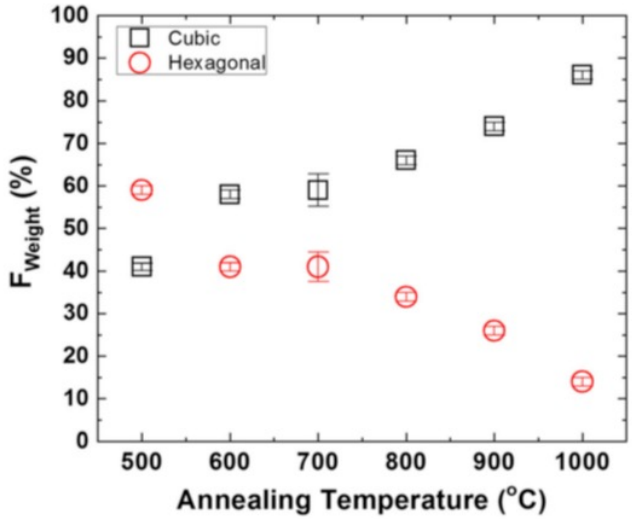

Figure 2 Weight fraction of the cubic and hexagonal phases versus annealing temperature for 2-h isothermal holds.

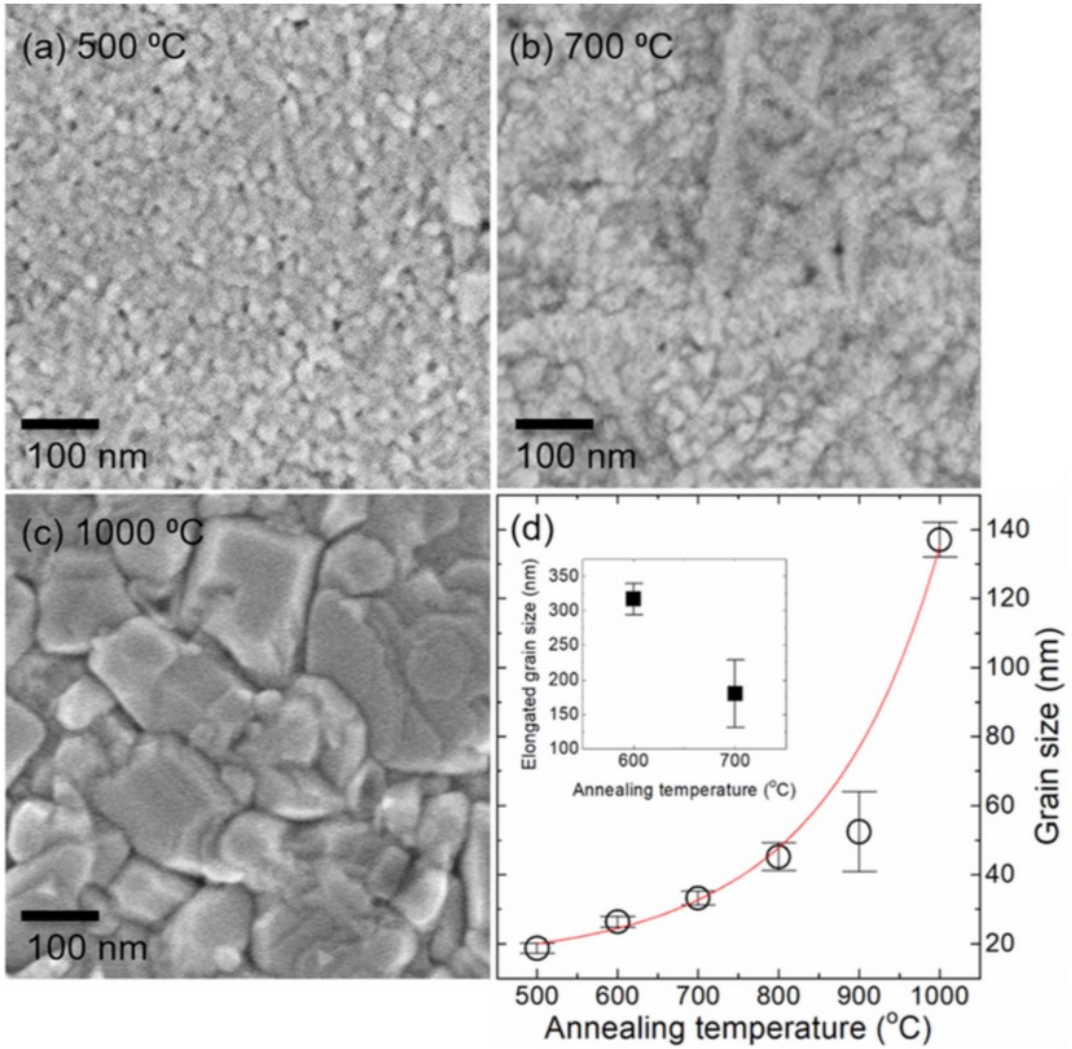

Figure 3 Surface images of $BaTiO_3$ thin films isothermally annealed at **a** 500 °C, **b** 700 °C and **c** 1000 °C, and **d** grain size variation versus annealing temperature.

Piezoelectric

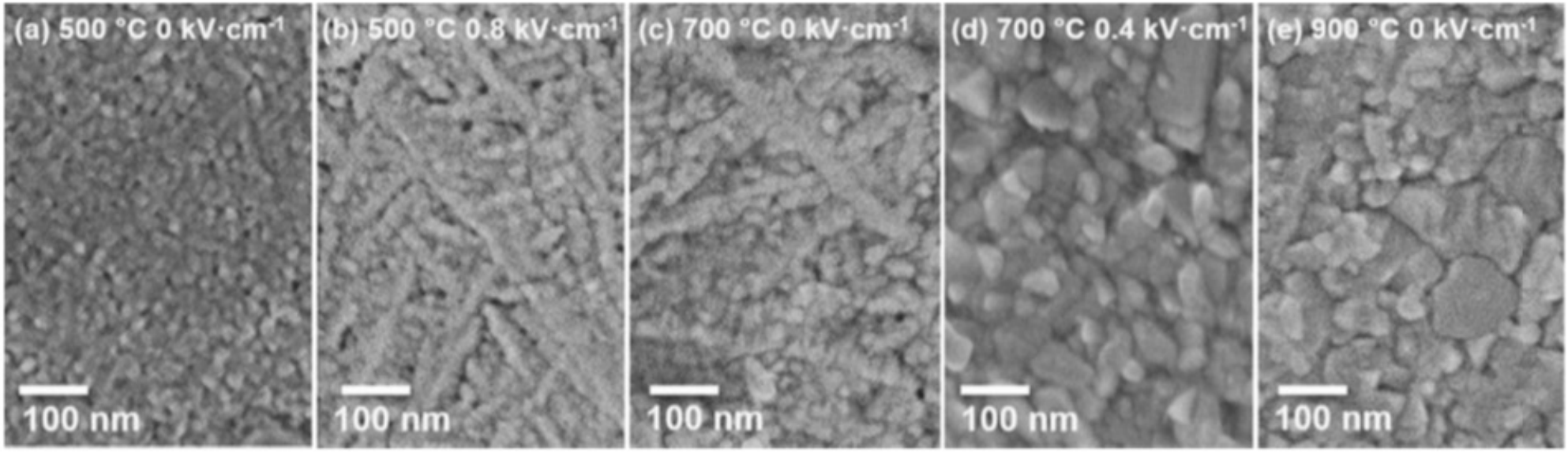

Figure 5 SEM images of $BaTiO_3$ thin films after a 2-h isothermal annealing. **a** 500 °C, 0 kV cm^{-1}, **b** 500 °C, 0.8 kV cm^{-1}, **c** 700 °C, 0 kV cm^{-1}, **d** 700 °C, 0.4 kV cm^{-1} and **e** 900 °C, 0 kV cm^{-1}.